J Solid State Electrochem (2005) 9: 205–233
DOI 10.1007/s10008-004-0568-z

ORIGINAL PAPER

G. Patermarakis · K. Moussoutzanis

Aluminium anodising in ultra-dense sulfate baths: discovery by overall kinetic and potentiometric studies of the critical role of interface colloidal $Al_2(SO_4)_3$ nanoparticles in the mechanism of growth and nanostructure of porous oxide coatings

Received: 15 March 2004 / Accepted: 13 May 2004 / Published online: 27 August 2004

Abstract The solubility of $Al_2(SO_4)_3$ in H_2SO_4 at different concentrations was determined and showed a minimum at ≈95% w/v. Overall kinetic and potentiometric studies of Al anodising were performed in large ranges of concentrations of saturated H_2SO_4 solutions and current densities. During anodising quasi-steady-state supersaturation and unsaturation conditions for concentrations below and above 95% w/v dominate in the pore-filling solution affecting those in the oxide–electrolyte interface. Interface colloidal $Al_2(SO_4)_3$ nanoparticles form occupying surface fractions increasing with salt concentration, supersaturation, field strength in the pore base surface and current density increase and temperature decrease. These control the mechanism and kinetics of growth and structural parameters of films and impose the growth of non-pitted uniform films up to current densities higher than in unsaturated baths, more effectively under supersaturation conditions. Well-defined peaks of structural parameters appear depending on thickness and current. Thus optimal regularly grown films of desired nanostructure and the introduction of new anodising technologies can be achieved.

Keywords Porous anodic aluminas · Ultra-dense sulfate baths · Interface colloidal $Al_2(SO_4)_3$ · Film growth mechanism · Nanostructure

Introduction

Porous anodic alumina films have a wide range of applications, for example in the improvement of mechanical properties of Al [1], as anticorrosion [2, 3, 4] and decorating [2, 3] coatings and membranes [5], in magnetic memories [6], in catalysis [7, 8, 9, 10, 11, 12, 13], etc. Owing to their nanometre-scale porous structure [2, 3, 7, 8, 9, 10, 11, 12, 13] and sizes of particles constituting the pore wall material [14], they have also recently found application in nanoscience and nanotechnology, for example in preparing oxide and then C nanotubes [15]. The optimisation of their effectiveness depends on the suitable design of their porous structure, nature/composition of pore wall oxide and their reactive properties. Porous anodic aluminas form in phosphoric, oxalic, chromic and sulfuric acid solutions [2, 3, 16, 17]. Bisulfates [18, 19] and mixtures of H_2SO_4 with sulfate salts have also been employed [18, 20, 21, 22, 23, 24, 25]; among these methods, H_2SO_4 has been employed most frequently.

The structure of uniformly/regularly grown porous anodic alumina films is defined by the surface density of pores, the diameter at their bases and the variation of diameter along them or the real pore shape. For films grown in H_2SO_4, the pore surface density, which is of the order of 10^{10} cm^{-2} [20], depends exclusively on, and decreases with, current density [20, 26]. The base diameter, varying from a few nm to a few tens of nm [20], depends on, and increases with, temperature and H^+ activity at pore bases [18, 26]. Pores open towards the surface due to the chemical dissolution of pore walls by the electrolyte during anodising [2, 27, 28, 29, 30, 31], similar to the open circuit oxide dissolution [27, 28, 29, 30, 31], which is a first-order reaction with respect to H^+ activity and is hindered by incorporated electrolyte anions [18]. For prolonged anodising, as a result of the opening up of pores [32, 33], a quasi-maximum limiting thickness may appear [2, 3, 32] which increases with current and decreases with temperature and H^+ activity.

When condensed $Al_2(SO_4)_3$ does not form inside the pores, low temperatures and electrolyte concentrations and high current densities favour the growth of low-porosity hard films [2, 3]. Sulfate salt additives like

G. Patermarakis (✉) · K. Moussoutzanis
School of Chemical Engineering,
Department of Materials Science and Engineering,
National Technical University, Iroon Polytechniou 9,
Zografou 157 80 Athens, Greece
E-mail: gpaterma@central.ntua.gr
Tel.: +30-210-7723099
Fax: +30-210-7723184

$Al_2(SO_4)_3$, $MgSO_4$, Na_2SO_4, $MnSO_4$, $(NH_4)_2SO_4$ and $NiSO_4$ [20, 21, 22, 23, 24] were also considered to favour hard films, since they are believed to reduce the solvent action of the electrolyte; however, their real effect was recently elucidated [18, 19, 25]. Their presence at relatively high H_2SO_4 concentration solutions may increase H^+ activity in some salt cases and always increases the concentration of incorporated anions. The former effect may thus increase the pore base diameter and rate of pore wall dissolution reaction, whereas the latter effect reduces that rate and its effect may prevail under some conditions.

Conditions discussed above [33, 34, 35] and sulfate additives (e.g. $Al_2(SO_4)_3$, $MgSO_4$ [21], and Na_2SO_4 [20]) also favour the appearance of pitting due to non-uniform/abnormal growth of film which excessively thickens at some surface positions [33, 34, 35]. Undesirable non-uniform aspects, thickness, porous structure, porosity, hardness, roughness and cracks appear. The recently elucidated mechanism and criteria for pitting appearance [34, 35] showed that hard films and pitting are together favoured. Unsolved problems for Al anodising technology are still the growth of regular films with desired (i) porosity low enough for mechanical applications or (ii) high surface density and base diameter of pores, thickness and real surface for applications involving reactive properties like adsorption and catalysis.

When condensed $Al_2(SO_4)_3$ forms, as recently shown [25], it appears as colloidal $Al_2(SO_4)_3$ micelles on the pore surface and their formation is catalysed by the field (pore base surface) and solid surface (pore base and wall surfaces). They together appear and dissolve, according to a quasi-equilibrium process, and affect the kinetics and mechanism of film growth by reducing the surface fraction of charge exchange and diameter at pore bases and the real fraction of wall surface where oxide dissolves and impose a mechanism of regular film growth. They appear on the surface of pores with nanometre-sized diameters. Their size is much lower than for example the pore base diameter and they are therefore nanoparticles. Their similar charge prevents coagulation and precipitate formation.

Al anodising in dense sulfate electrolytes thus appears attractive and promising. Saturated electrolytes are the most important, since they evidently favour more appearance of micelles. Different salts can be used but the most convenient is $Al_2(SO_4)_3$ which is identical to that produced inside pores. It seems that anodising in $H_2SO_4 + Al_2(SO_4)_3$ saturated baths at largely varying H_2SO_4 concentrations can yield: (i) further details to help elucidate the critical role of micelles in the mechanism of oxide growth; (ii) discovery of the main parameters determining their critical role; and (iii) optimisation of film growth as regards several structural properties. A combined overall kinetic and potentiometric method [18, 25] was applied in this study that constitutes an effective tool to penetrate into the phenomena occurring at the barrier layer and pore walls during anodising where other methods (i.e. those used for barrier-type films) are ineffective, inaccurate or inapplicable due to the existence of pores.

Experimental

In order to choose suitable anodising electrolyte solutions the solubility of $Al_2(SO_4)_3$ in H_2SO_4 was first determined. Solutions of $H_2SO_4 + Al_2(SO_4)_3$ were prepared at different concentrations; increments of 0.0167 and 0.0083 mol dm^{-3} $Al_2(SO_4)_3$ concentration were employed around the saturation concentration in the regions of higher and lower solubilities, respectively. The solutions were thermostated at 35°C and vigorously agitated for 30 min and then left to relax successively at 30, 25 and 20°C for approximately 48 h at each temperature. The lowest concentration at which distinguishable crystals first appeared was considered to be the $Al_2(SO_4)_3$ solubility; this was thus determined with an error of ± 0.0167 or ± 0.0083 mol dm^{-3}.

Al sheets 0.5-mm thick and 99.5% pure were used. The Al composition, the shape and dimensions of Al anodes and Pb cathodes used and the procedure for the washing and neutralization of Al specimens after anodising to remove H_2SO_4 and $Al_2(SO_4)_3$ from pores and drying are described elsewhere [32]. The washing of anodised specimens with water and their neutralization with 0.1 mol dm^{-3} NaOH are generally performed within a few minutes at room temperature [32]; however, in this case, washing and neutralization were performed at 35°C for a longer time, 10 min, to remove all the solvable species. The specimens were then dried in an air stream and placed in a desiccator for 24 h.

Anodic oxidation of Al was performed galvanostatically in thermostated and vigorously agitated saturated H_2SO_4 15–105% w/v + $Al_2(SO_4)_3$ solutions at temperatures of 20, 25 and 30°C and current densities of 15, 35, 55, 75, 105 and 135 mA cm^{-2} which thus extend from low to high enough values.

During galvanostatic anodising and thickening of the anodic film after the initial stages, the anodising voltage required to keep constant current always increases. For all H_2SO_4 concentrations, except 45% w/v, and current densities the required increase of voltage continued up to near 50 V; then, anodising was interrupted. At 45% w/v, anodising continued up to about 50 V for current densities of 35, 55 and 75 mA cm^{-2} but at 15, 105 and 135 mA cm^{-2} voltage values did not reach 50 V even for prolonged anodising (see later). Different times were employed up to those corresponding to the final voltage values.

The anodic potential, determined as described previously [36], which almost coincides with the potential drop across the barrier layer [18] is close to the anodising voltage. For convenience the latter was recorded. The film masses were found as described previously [33]. Anodised specimens were examined macroscopically and by microscope as described earlier [34] to reveal the presence or absence of pitting.

Results

Solubility of $Al_2(SO_4)_3$ in H_2SO_4 solutions: choice of suitable electrolyte compositions

The concentration of $Al_2(SO_4)_3$ ($C_{s,0}$) corresponding to solubility ($C_{s,s}$) in solutions of different H_2SO_4 concentrations ($C_{a,0}$) and at different temperatures (T) is shown in Fig. 1. A minimum appears ($C_{s,s,m}$) around $C_{a,0} \approx 95\%$ w/v $= C_{a,0,m}$ at all T values. Temperature seems to exert some positive effect on the solubility. The application of saturated $H_2SO_4 + Al_2(SO_4)_3$ solutions at a low $C_{a,0}$ (i.e. 15% w/v), at $C_{a,0}$ values below and above $C_{s,s,m}$ but not largely differing from $C_{s,s,m}$ and at an intermediate value between the lower and the first of the above is expected to yield significant information for the subject under consideration. Thus, the $C_{a,0}$ values of 15, 45, 85 and 105% w/v (or 1.53, 4.59, 8.67 and 10.71 mol dm^{-3}) H_2SO_4 solutions were chosen. The added $Al_2(SO_4)_3$ corresponded to concentrations 0.750, 0.270, 0.083 and 0.167 mol dm^{-3}, respectively, for these $C_{a,0}$ values, and were slightly higher than the saturation ones. The small amount of precipitate did not appreciably hinder bath stirring whilst always assuring a saturated bulk solution.

Potentiometric studies: dependence of anodising voltage on time, film thickness, current density and temperature

The anodising voltage (ΔV) varies with time (t) at different current densities (j) and T values as shown in Fig. 2a–f. As observed, within a t of the order of 1 s, ΔV rises abruptly up to a value depending on j and $C_{a,0}$. Then, during a transient period (extending from a time < 0.5 up to ≈ 4 min) which decreases with j and T and $C_{a,0}$ up to 85% w/v after which it rises, ΔV diminishes and a minimum appears (ΔV_m). At $t > t(\Delta V_m)$ and the lower j, ΔV increases with t initially moderately or slightly and later strongly for $C_{a,0} = 15$, 45 and 85% w/v, while it increases moderately at $C_{a,0} = 105\%$ w/v. At higher j values a strong accelerated increase occurs which may be followed by details towards the higher t values in some cases.

As previously noted at $C_{a,0} = 45\%$ w/v and the two higher j values employed, the final ΔV values were < 50 V. In both cases pitting appeared on the surface during the initial stages [34, 35] while large pitting areas (burning) [34] were observed, accompanied by a characteristic noise, in a few cases at 105 mA cm^{-2} usually in the corners of specimens and always at 135 mA cm^{-2}, except probably a case of a film prepared at $t = 20$ min, either in the corners or most frequently around the

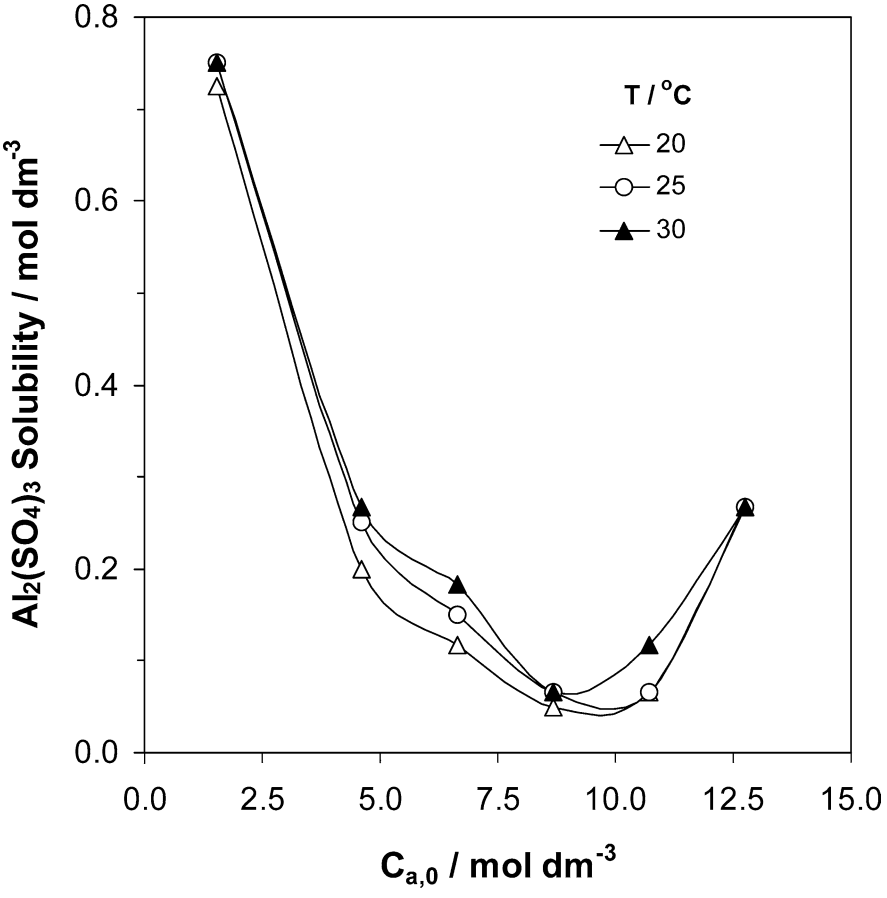

Fig. 1 Variation of $Al_2(SO_4)_3$ solubility ($C_{s,s}$) in H_2SO_4 solution with H_2SO_4 concentration ($C_{a,0}$) at different temperatures (T)

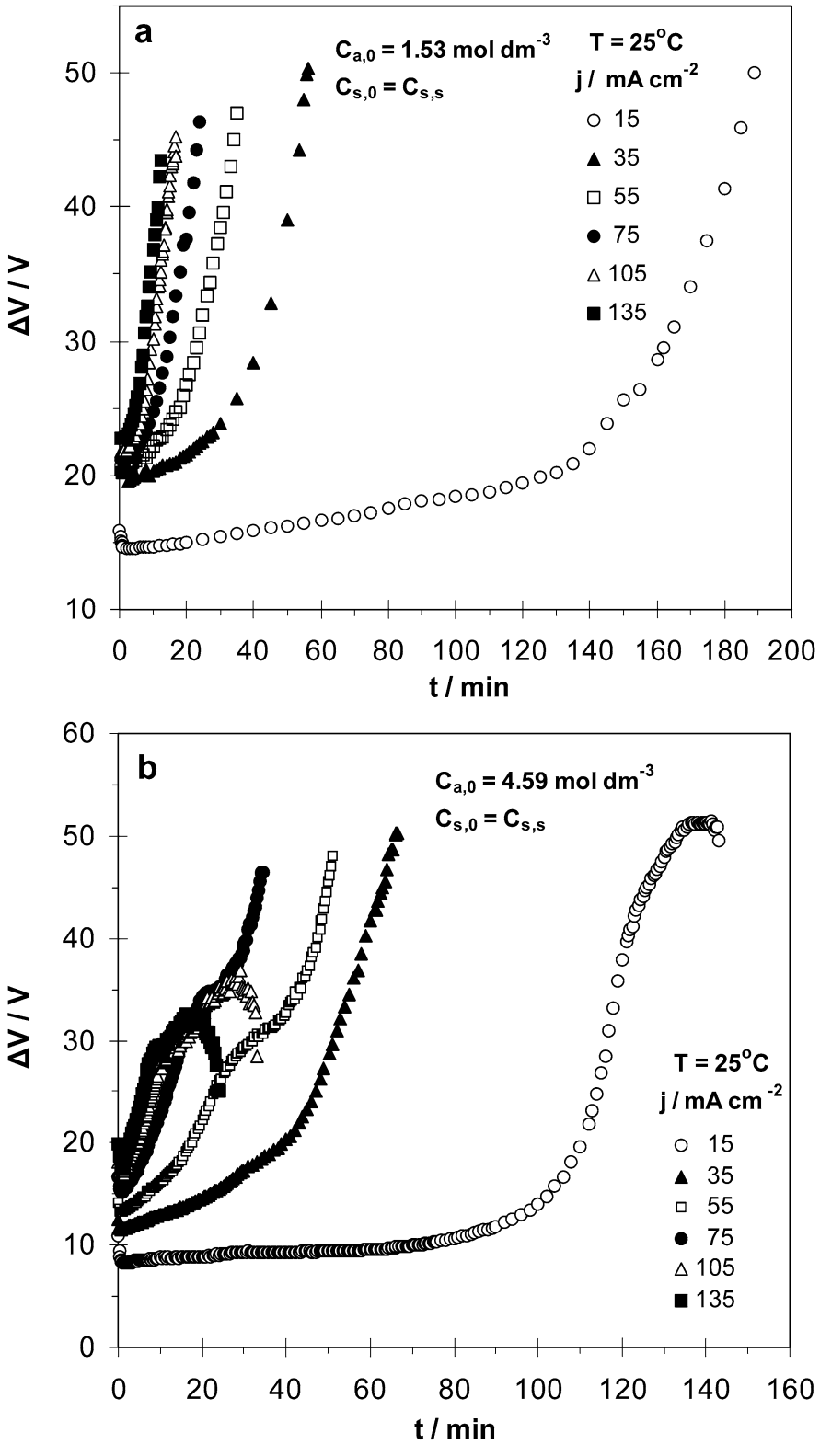

Fig. 2 Variation of the anodising voltage (ΔV) with time (t) at different H_2SO_4 concentrations ($C_{a,0}$), current densities (j), bath temperatures (T), and at saturation $Al_2(SO_4)_3$ concentrations ($C_{s,0} = C_{s,s}$)

middle of the lower specimen side. But in both cases at high enough t values and before ΔV reaches 50 V, burning developed anyway around the middle of the lower specimens' side causing damage (i.e. gradual consumption of metal and then a decrease of its geometric surface, etc.). Also, successive maxima and minima and other chaotic details in the ΔV vs. t plots appeared. These are attributed to the fact that a flood of current passes through the burning region where temperature excessively rises, and the current in the remaining surface

Fig. 2 (Contd.)

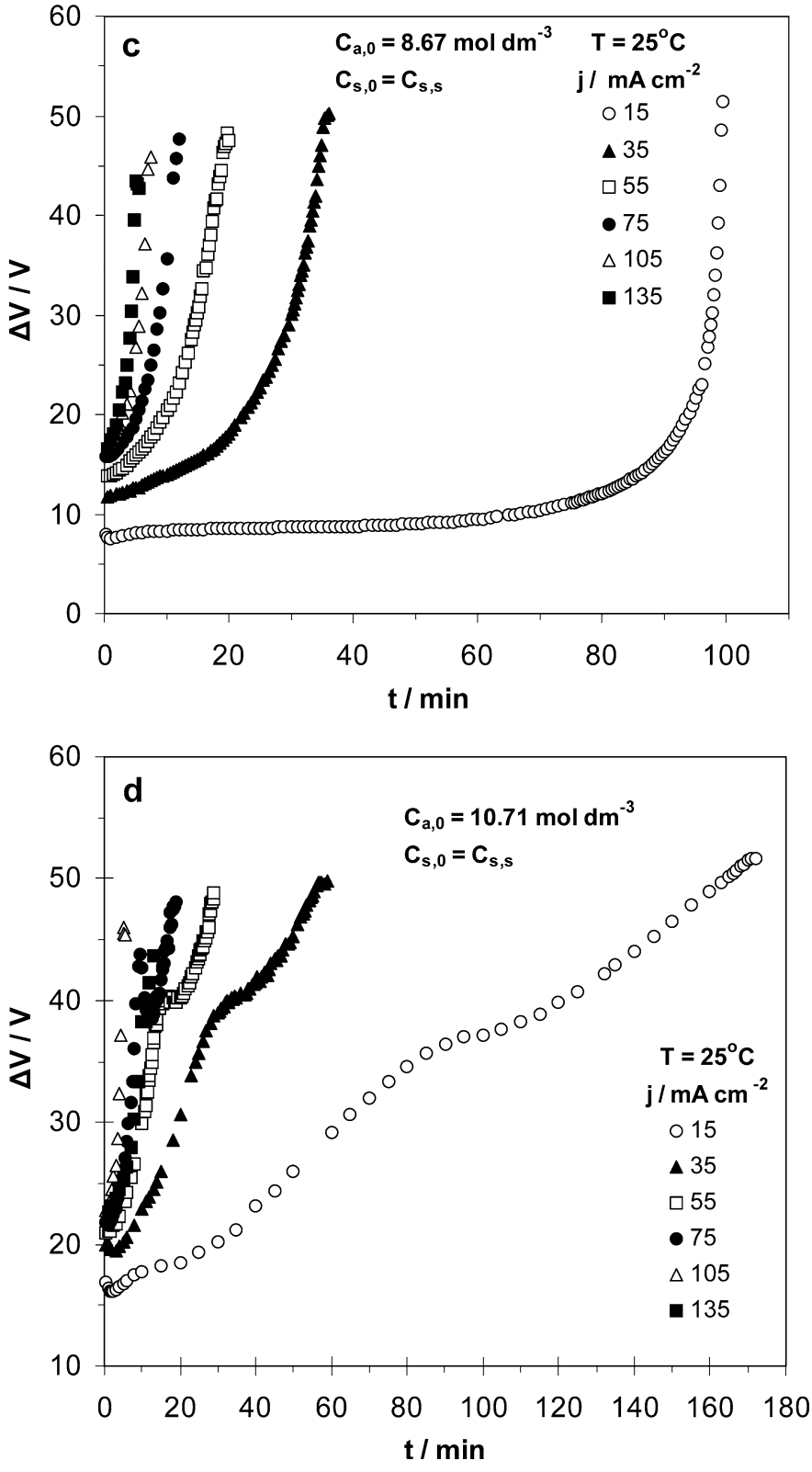

regions decreases drastically; both parameter changes cause a decrease in the necessary ΔV value [36], while the solution around the burning region may become unsaturated, so that the control of oxide growth by $Al_2(SO_4)$ micelles (see later) weakens. This distribution of current, temperature and other related structural and kinetic parameters in the specimen surface is unstable yielding the observed maxima, minima and other chaotic details.

At $C_{a,0} = 45\%$ w/v and the lower j value at prolonged enough anodising a maximum appeared in the ΔV vs.

Fig. 2 (Contd.)

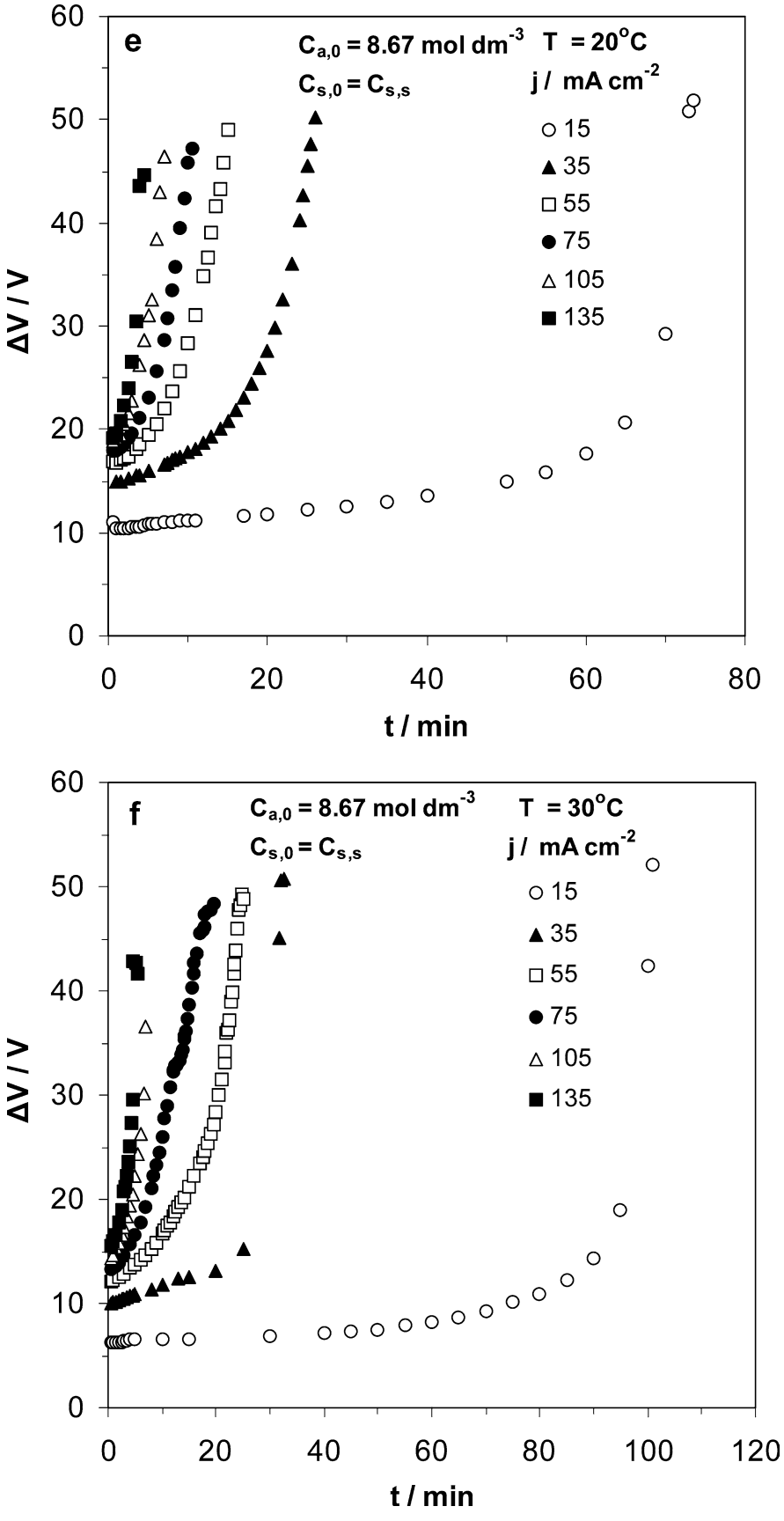
e
$C_{a,0}$ = 8.67 mol dm^{-3} T = 20°C
$C_{s,0}$ = $C_{s,s}$
j / mA cm^{-2}
15
35
55
75
105
135
ΔV / V
t / min
f
$C_{a,0}$ = 8.67 mol dm^{-3} T = 30°C
$C_{s,0}$ = $C_{s,s}$
j / mA cm^{-2}
15
35
55
75
105
135
ΔV / V
t / min

t plot. At $C_{a,0} = 105\%$ w/v the plots at $t > t(\Delta V_m)$ have a sigmoidal profile with a main inflection point at low j values, but at higher j values they show successively a maximum, a minimum and an inflection point. The origins of these characteristic features of plots in the latter two cases are generally different from those at $C_{a,0} = 45\%$ w/v and the two higher j values.

The thickness of uniformly/regularly developed films or the average one of irregularly grown films (h) is given by the following equation:

$$h = \mathrm{k'}t = \mathrm{k''}jt,\ (t \leqslant t_I) \tag{1}$$

where $\mathrm{k''} = 3.09\times10^{-6}$ cm^3 mA^{-1} min^{-1} (i.e. it is a constant) and t_l is the time up to which h increases linearly with t [32]. The time t_l is identical to, or slightly higher than, t_m at which the maximum average pore diameter near or at film surface approaches first the cell width and the surface appearance starts to change from shiny transparent and similar to Al metal to a mat, milky one [32, 33, 34]. For $t > t_l$, h increases with t with a decreasing rate up to t_c at which point the rate may become approximately zero; a (quasi) maximum limiting h (h_c) may then be achieved exceeding slightly or appreciably $\mathrm{k''}jt_m$ or $\mathrm{k''}jt_l$ [32, 33].

Since t_l cannot be easily and accurately determined, oppositely to t_m, the t_m and $h(t_m)$ values were considered. At $C_{a,0} = 15\%$ w/v ($T = 25$°C) and $j = 15$ mA cm^{-2}, $t_m \approx 120$ min; at all other j values the higher t employed was $\leq t_m$. At $C_{a,0} = 45\%$ w/v ($T = 25$°C), $t_m \approx 45$, 40, 27.5, 20, 15 and 10 at the employed j values. At $C_{a,0} = 85$ w/v and $T = 20$°C, $t_m \approx 50$, 25, >15, 10, 7 and 4.5 min; at $T = 25$°C, $t_m \approx 40$, 30, 20, >12.5, >7.5 and 5 min; and at $T = 30$°C, $t_m \approx 20$, 20, 15, 12.5, 7.5 and 5 min. At $C_{a,0} = 105\%$ w/v ($T = 25$°C), $t_m \approx 50$, 30, 12.5, 8, >5 and 2.5 min. At $C_{a,0} = 105\%$ w/v, t_m is close to the lower t at which a first inflection point before the main one (low j values) or the maximum (high j values) of ΔV vs. t plot appears. The $h(t_m)$ values were found from Eq. (1). By using Eq. (1), the ΔV vs. h [$h \leq h(t_m)$] plots were constructed, Fig. 3a–f, the relative positions of which differ significantly from those of ΔV vs. t plots, especially at high j values. These plots are important for disclosing the critical role of $Al_2(SO_4)_3$ micelles in the film growth mechanism (see later).

Overall kinetic study

Variation of film mass with t, h, j, T and $C_{s,0}$

The plots of film mass (m) spread over the entire anodised geometric surface of Al specimens ($S_g = 30.75$ cm^2 [32, 33]) vs. t are given in Fig. 4a–f. The m vs. h [$h \leq h(t_m)$] plots are given in Fig. 5a–f.

Overall kinetic models of oxide growth

At $C_{s,0} = 0$ and constant j, when the growth of film is regular and the diameter of pores at their bases (D_b) remains constant during anodising, the ΔV vs. t plot shows an almost horizontal plateau for $t > t(\Delta V_m)$ [34]. Then, the following kinetic model applies [33, 34] irrespective of the real pore shape [32, 33]:

$$A = (\mathrm{k}jt - m)\left(4^{-1}\pi S_g d_c \mathrm{k'}t\right)^{-1} = A_0 + A_1 t + A_2 t^2 = 4\pi^{-1}p,\ [A_0, A_1, A_2 > 0 \text{ and } t(\Delta V_m) \leqslant t \leqslant t_m] \tag{2}$$

where A is a dimensionless factor, k is a constant resulting from Faraday's law, S_g is the geometric surface area of Al specimens, d_c is the density of compact pore wall oxide (3.42 g cm^{-3}) [32], A_0 equals nD_b^2 where n is the surface density of pores and D_b is the pore base diameter, A_1 and A_2 are parameters depending on j and T and p is porosity (v/v). From Eq. (1), Eq. (2) becomes

$$A = A_0 + A_1' h + A_2' h^2 = 4^{-1}\pi p,\ \left[A_0, A_1', A_2' > 0 \text{ and } h[t(\Delta V_m)] \leqslant h \leqslant h(t_m)\right]. \tag{3}$$

For $t = 0$ the model (2) gives $A_0 = 4\pi^{-1}p$ but initially only a barrier layer exists with zero porosity. Evidently it applies after the t of pore nucleation, which is of the order of 1 s [18], i.e. negligible compared to the $t(\Delta V_m) \approx 0.5$–4 min. The limitation $t(\Delta V_m) \leq t \leq t_m$ satisfies that condition. The A (or p) parameter is related to basic parameters like n, D_b, etc., and magnifies the m differences permitting detailed/accurate studies of regular film growth [18, 26, 33].

When ΔV increases significantly with t, some scatter of points is usually observed and the A vs. t [$t(\Delta V_m) \leq t \leq t_m$] and $h\{h[t(\Delta V_m)] \leq h \leq h(t_m)\}$ plots at $C_{s,0} = C_{s,s}$ obey the following equation [25]:

$$A \approx A_0 + A_1 t + A_2 t^2 = A_0 + A_1' h + A_2' h^2 \tag{4}$$

where A_0, A_2 and A'_2 are >0 while A_1 and A'_1 are usually >0 at low j values and gradually become <0 at high j values and minima appear. In this case the mechanism of film growth embraces the appearance of colloidal $Al_2(SO_4)_3$ nanoparticles on pore surface (at least at pore bases) and D_b decreases with t or h [25]. As A_1 (or A'_1) becomes lower, D_b decreases faster with t or h and/or the average rate of pore wall chemical dissolution diminishes, both due to the rise of surface fraction occupied by them.

The A vs. h plots are given in Fig. 6a–f. Taking into account Fig. 2, all plots in Fig. 6 meet this case. The above parameter values appear in Table 1. The solutions are saturated, and $Al_2(SO_4)_3$ micelles must always form on the whole pore wall surface to the highest possible extent. For each $C_{a,0} \leq 85\%$ w/v, the plot is shifted down and turned to the right while the span of A values decreases as j increases up to ≈ 75 mA cm^{-2}; an imperceptible exception is only observed at $C_{a,0} = 45\%$ w/v in the region of high h values where the plots at $j = 55$ and 75 mA cm^{-2} intersect each other rather due to experimental errors. For $C_{a,0} = 105\%$ w/v these occur up to $j \approx 35$ mA cm^{-2}. For higher j values the trends for plot shift and the span of A variation with j change.

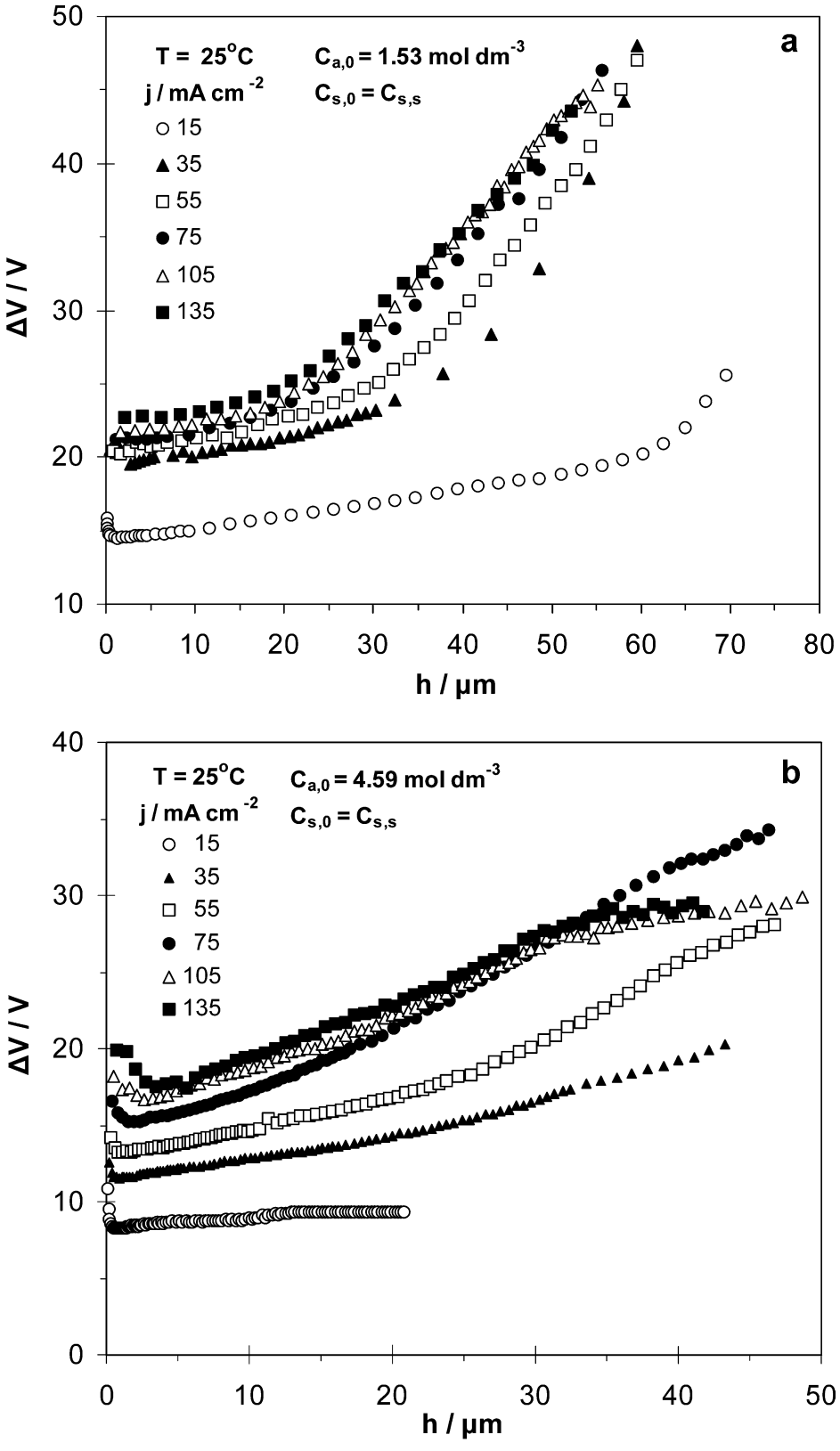

Fig. 3 Variation of the anodising voltage (ΔV) with film thickness ($h[h \leq h(t_m)]$) at different H_2SO_4 concentrations ($C_{a,0}$), current densities (j), bath temperatures (T), and at saturation $Al_2(SO_4)_3$ concentrations ($C_{s,0} = C_{s,s}$)

Dependence of A (or p) on $C_{a,0}$ at different h and j values

The A vs. $C_{a,0}$ plots at $T = 25°C$ and different h and j values are given in Fig. 7a–f. It is observed that at all j values $A(h \to 0) = A_0$ passes through a maximum usually around $C_{a,0} = 45\%$ w/v or in the region from 45% to 85% w/v. For higher h values, as h increases, complex trends for the

Fig. 3 (Contd.)

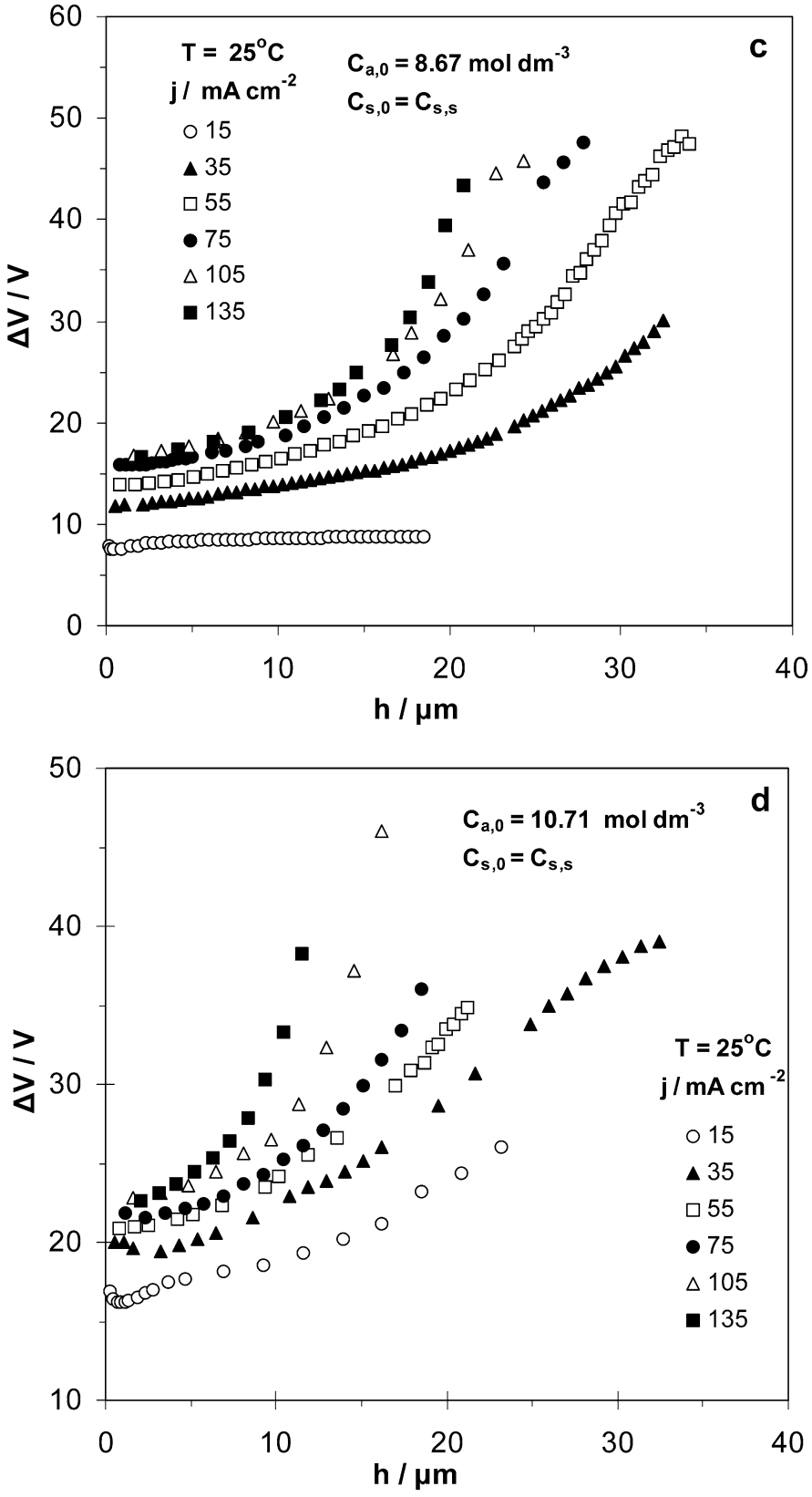

variation of the shape of plots and their relative positions depending on j are observed. Since n depends only on j [25], at each j comparable A values when $h \to 0$ (or A_0) point out comparable D_b values ($h \to 0$) while the variation of A_0 reflects the variation of D_b ($h \to 0$). The plots of Fig. 7, as well as those of Fig. 6, are also important for disclosing the critical role of $Al_2(SO_4)_3$ micelles in the film growth mechanism (see later).

Fig. 3 (Contd.)

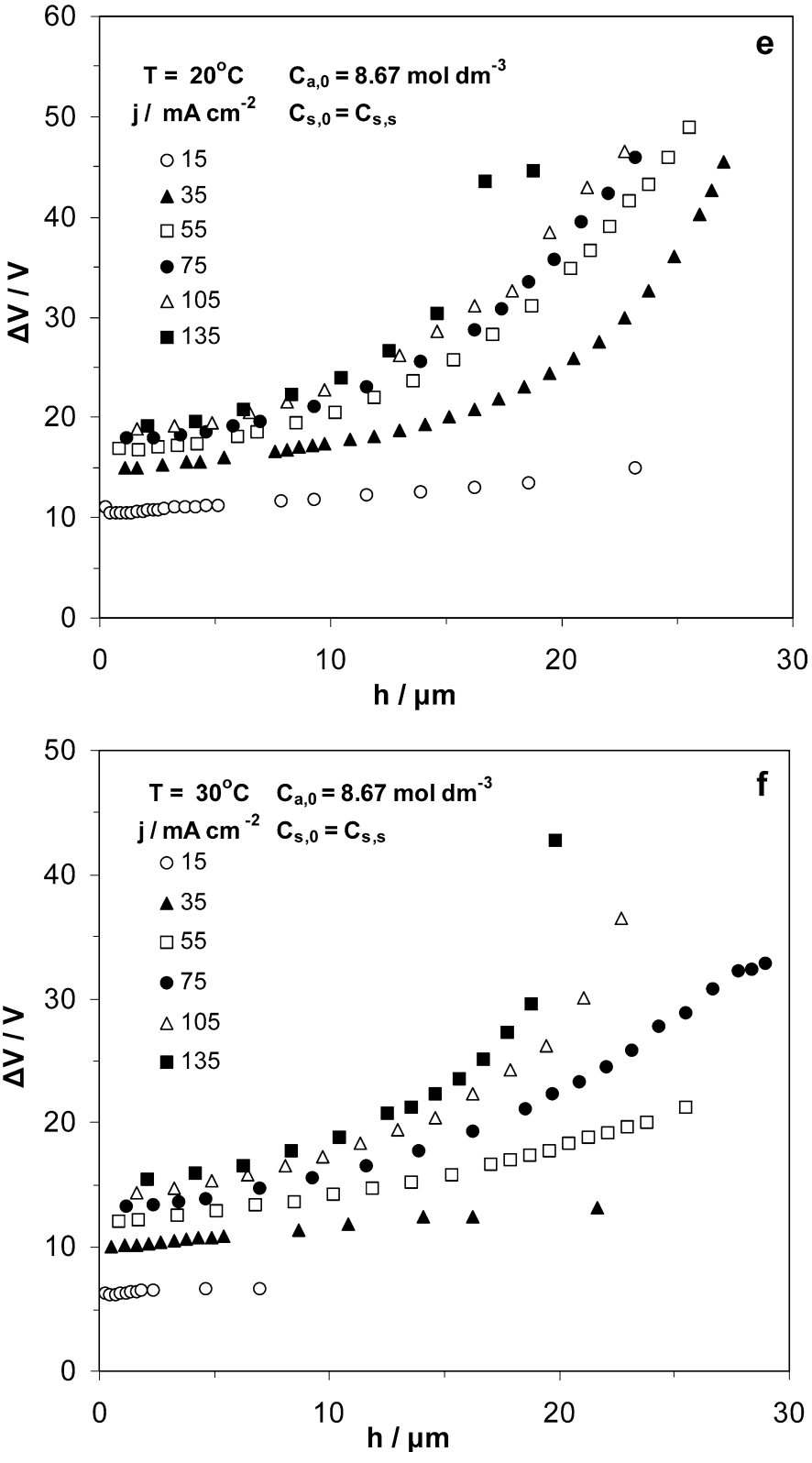

Conditions of regular film growth

Pitting, as described elsewhere [33, 34], was detected at $t \leq t_m$ for $j \geq 75$ mA cm^{-2} at $C_{a,0} = 15$ and 45% w/v. It was more intensive at 45% w/v and capable of causing damage to specimens on prolonged anodising, as already noted. At the other $C_{a,0}$ values and all T values employed, pitting was not detected even up to $j = 135$ mA cm^{-2}. It is noted that in films prepared at $C_{s,0} = 0$, $T = 25$°C and $C_{a,0} = 15$ and 45% w/v, pitting

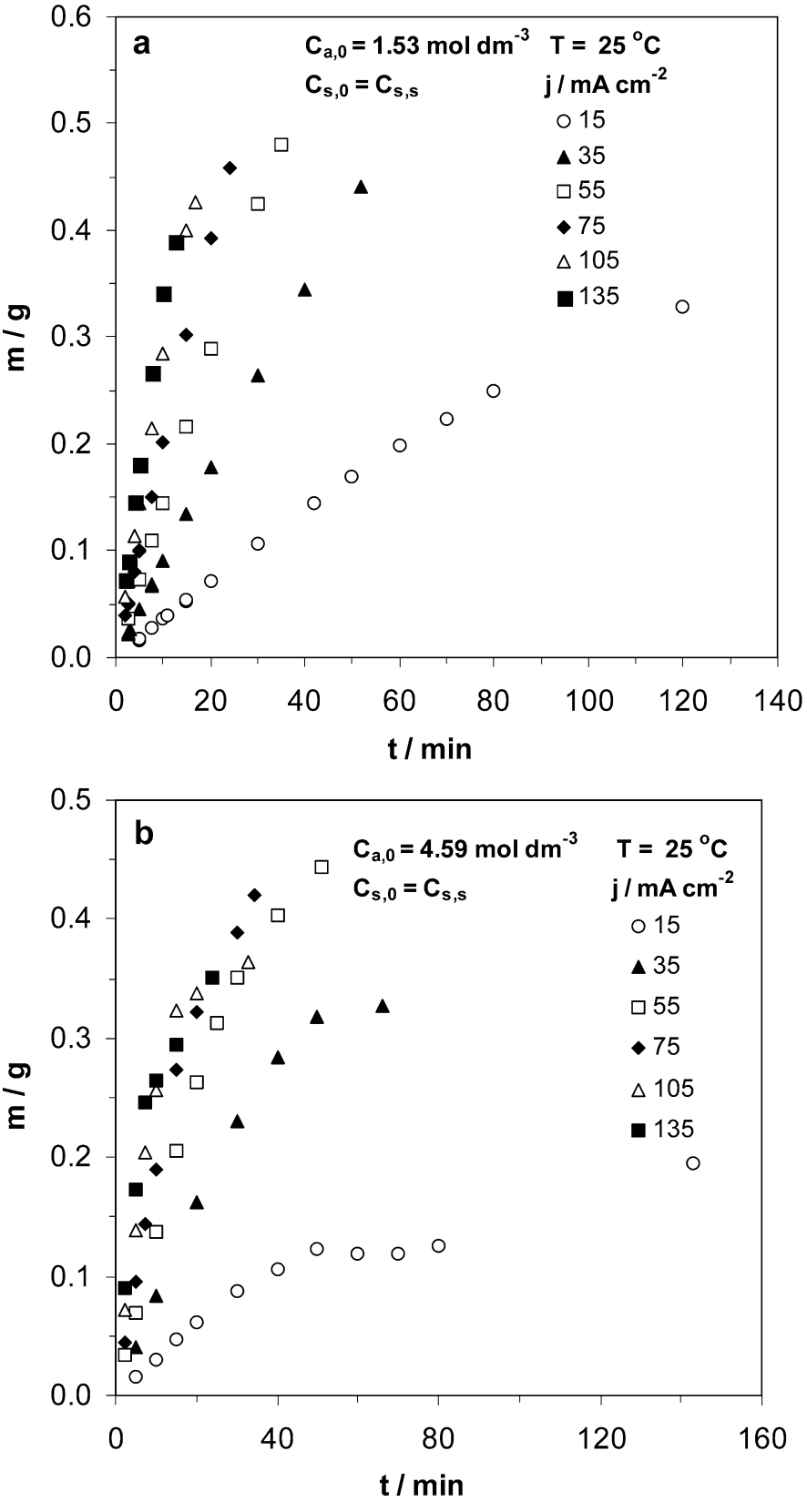

Fig. 4 Variation of the film mass (m) spread over the entire anodised geometric surface area of the Al specimens 30.75 cm^2 with time (t) at different H_2SO_4 concentrations ($C_{a,0}$), current densities (j), bath temperatures (T), and at saturation $Al_2(SO_4)_3$ concentrations ($C_{s,0} = C_{s,s}$)

was observed at $j \geq 25$ and a little > 35 mA cm^{-2}, respectively [29]; thus these limiting j values are much higher for films prepared at $C_{s,0} = C_{s,s}$. At the higher $C_{a,0}$ values employed the relevant j values at $C_{s,0} = 0$ are expected to be lower but not strongly different than those at $C_{s,0} = C_{s,s}$ as a result of the low $C_{s,s}$

Fig. 4 (Contd.)

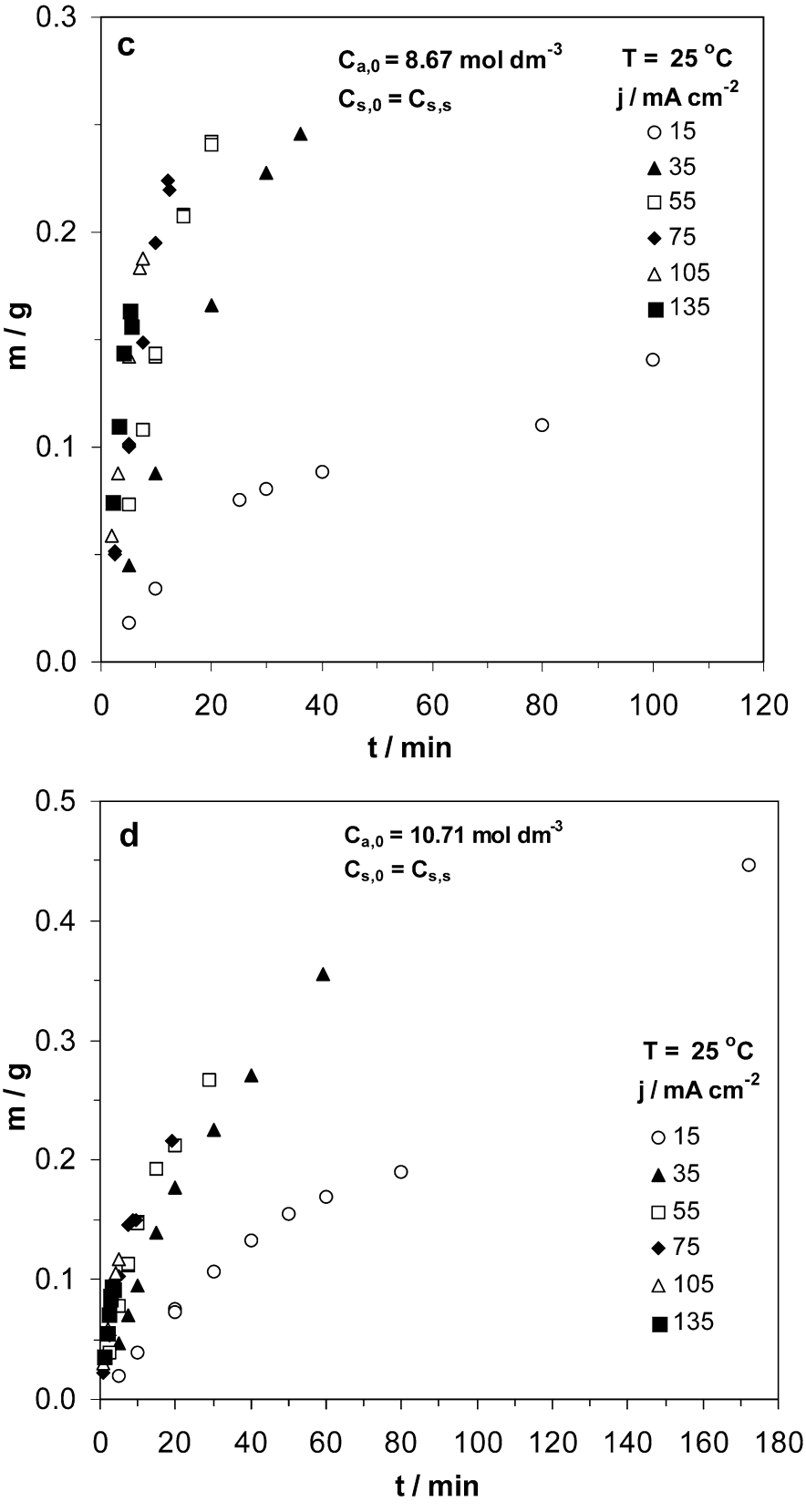

values. As noted elsewhere [25], this limiting j decreases with $C_{s,0}$ up to a $C_{s,0}$ value up to which micelles do not form on the pore base surface. For higher $C_{s,0}$ values the j limit strongly increases with $C_{s,0}$ as a result of the enhanced formation of micelles, and becomes highest at $C_{s,0} = C_{s,s}$; this j limit is greater

Fig. 4 (Contd.)

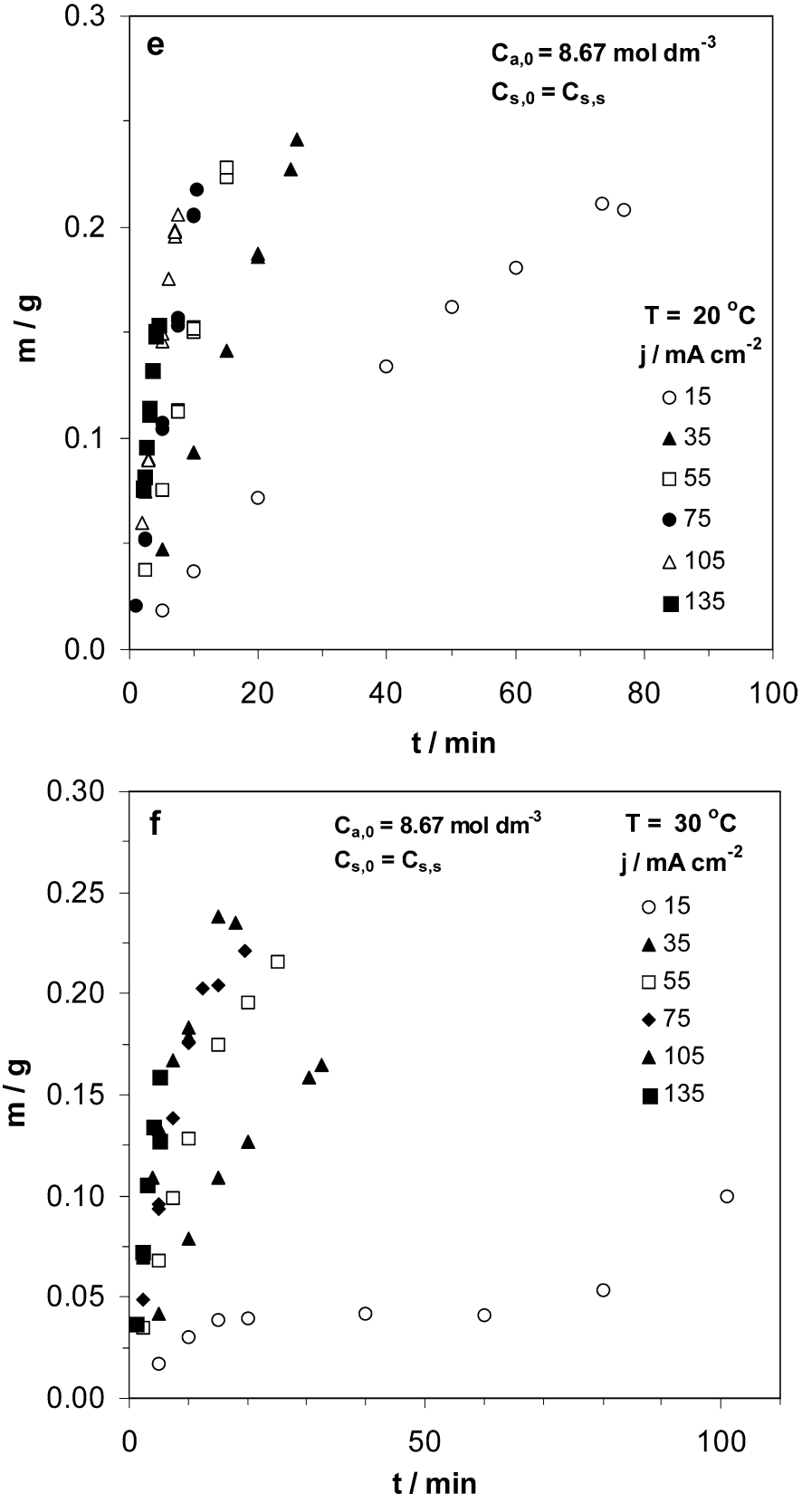

than that at $C_{s,0}=0$. The higher j limit at $C_{s,0}=C_{s,s}$ than at $C_{s,0}=0$ is thus justified. Citation of photographic/microphotographic material of pitted surfaces was judged unnecessary, since they were generally similar to those appearing elsewhere [33, 34] and would add no new significant information.

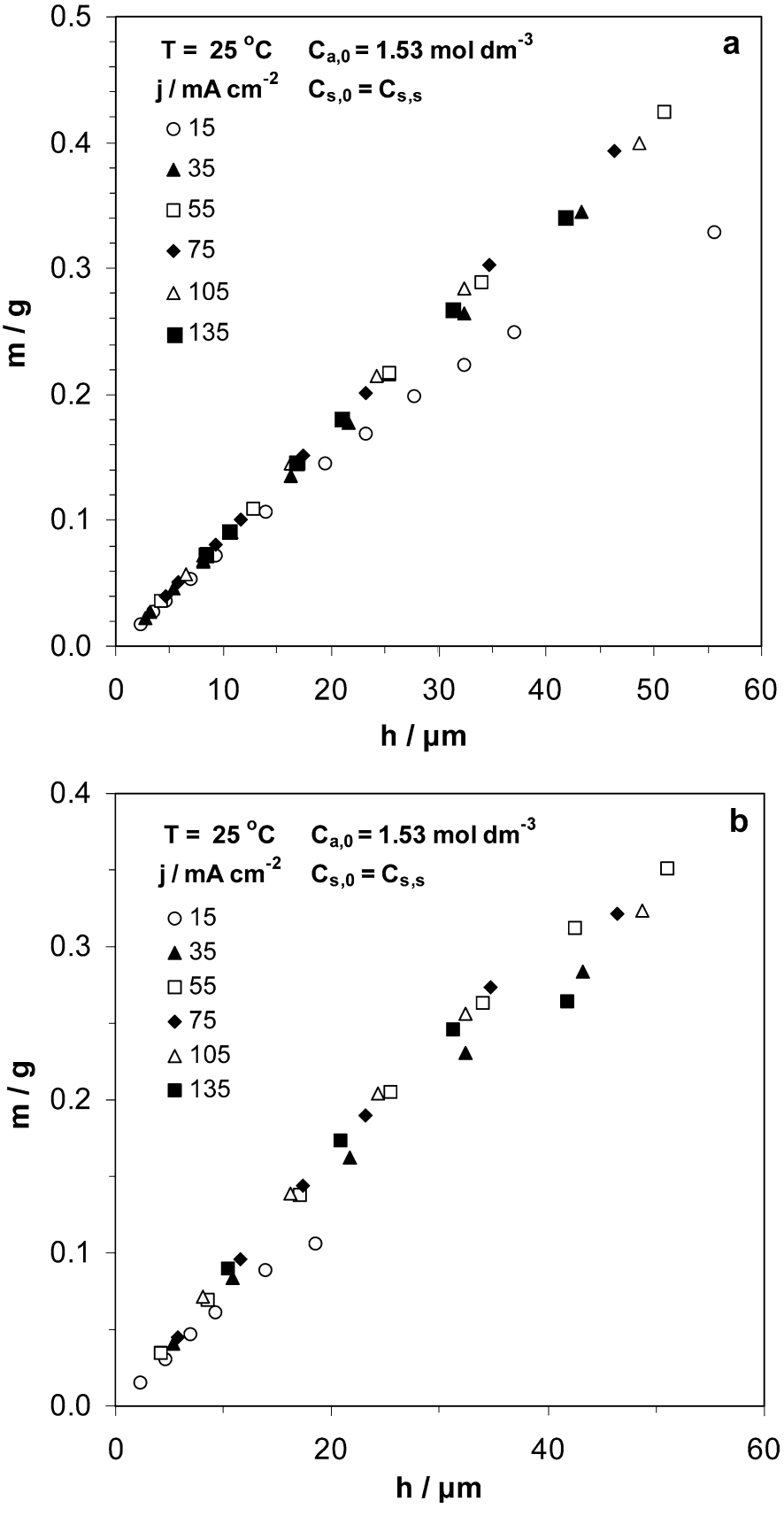

Fig. 5 Variation of the film mass (m) spread over the entire anodised geometric surface area of the Al specimens 30.75 cm^2 with film thickness ($h[h \leq h(t_m)]$) at different H_2SO_4 concentrations ($C_{a,0}$), current densities (j), bath temperatures (T), and at saturation $Al_2(SO_4)_3$ concentrations ($C_{s,0} = C_{s,s}$)

Fig. 5 (Contd.)

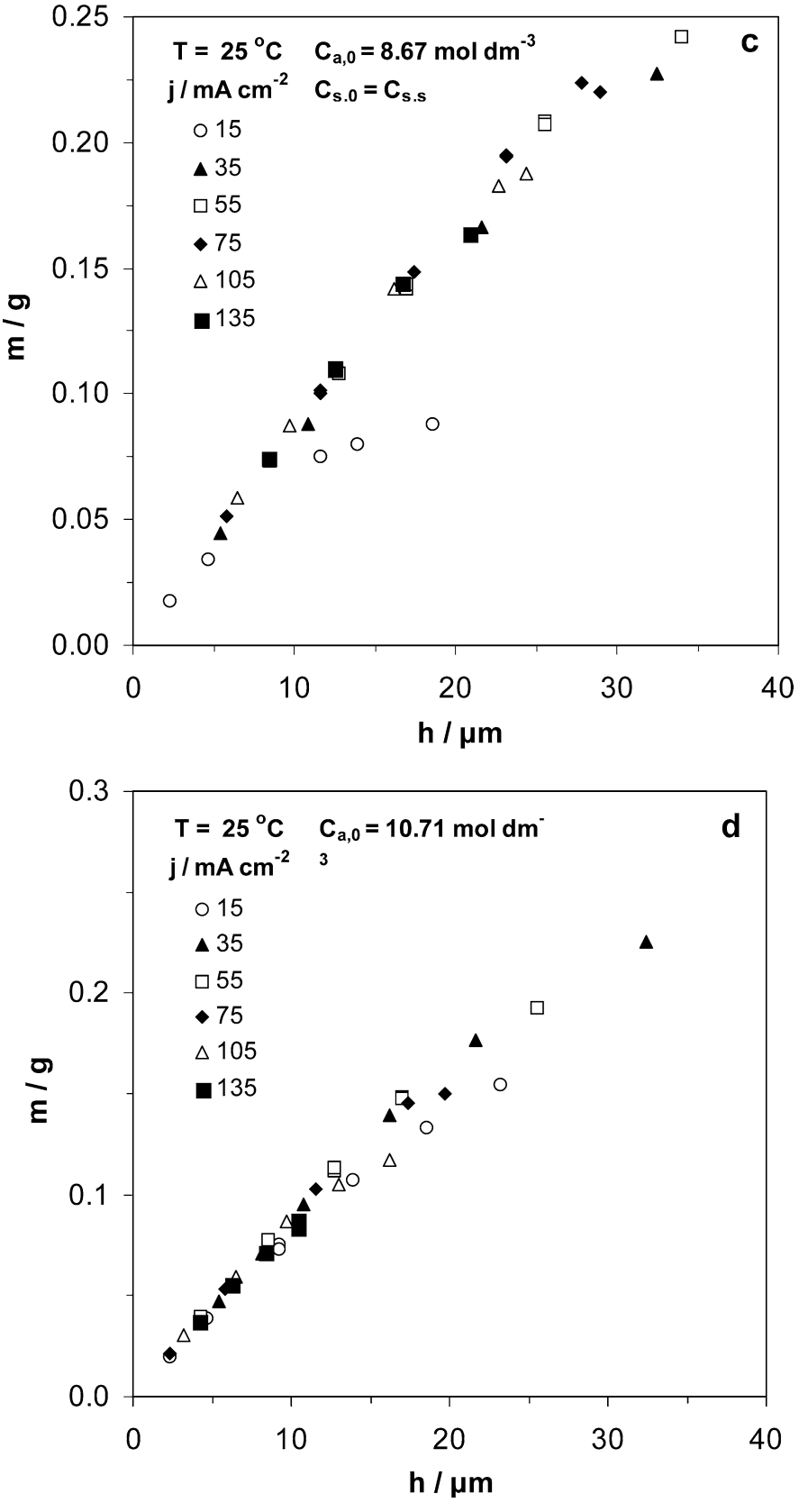
T = 25 °C
$C_{a,0}$ = 8.67 mol dm^{-3}
j / mA cm^{-2}
$C_{s.0}$ = $C_{s.s}$
c
15
35
55
75
105
135
m / g
h / µm
0.00
0.05
0.10
0.15
0.20
0.25
0
10
20
30
40
T = 25 °C
$C_{a,0}$ = 10.71 mol dm^{-3}
j / mA cm^{-2}
d
15
35
55
75
105
135
m / g
h / µm
0.0
0.1
0.2
0.3
0
10
20
30
40

Fig. 5 (Contd.)

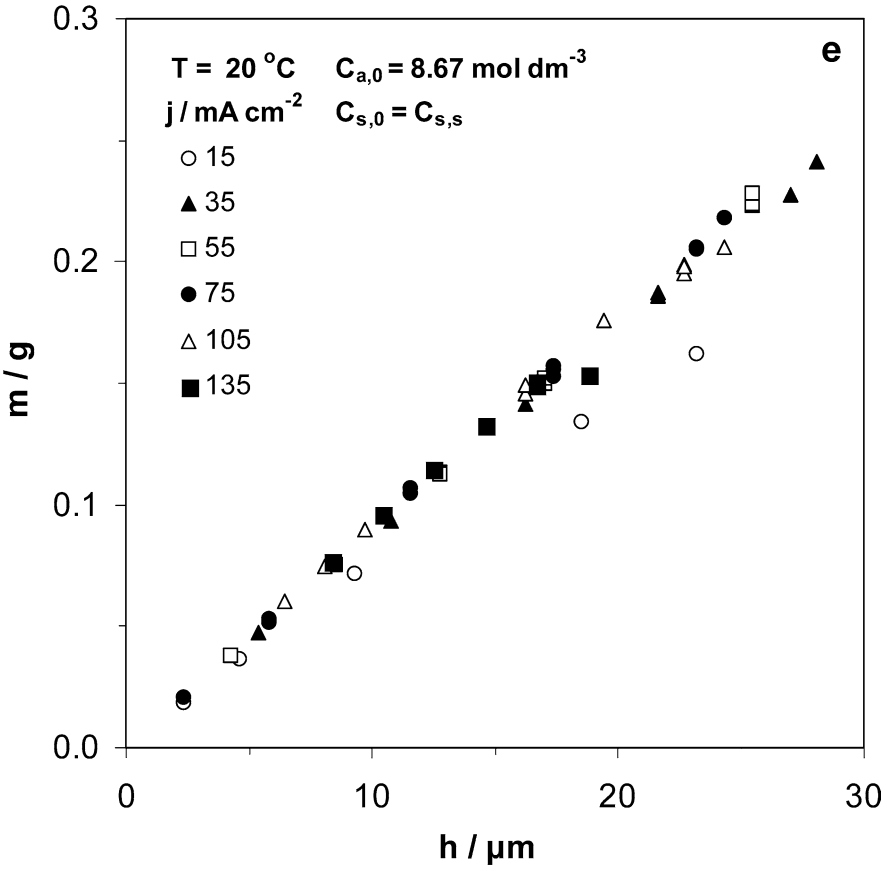
T = 20 °C
$C_{a,0}$ = 8.67 mol dm^{-3}
j / mA cm^{-2}
$C_{s,0}$ = $C_{s,s}$
15
35
55
75
105
135
e
m / g
h / µm
0.0
0.1
0.2
0.3
0
10
20
30

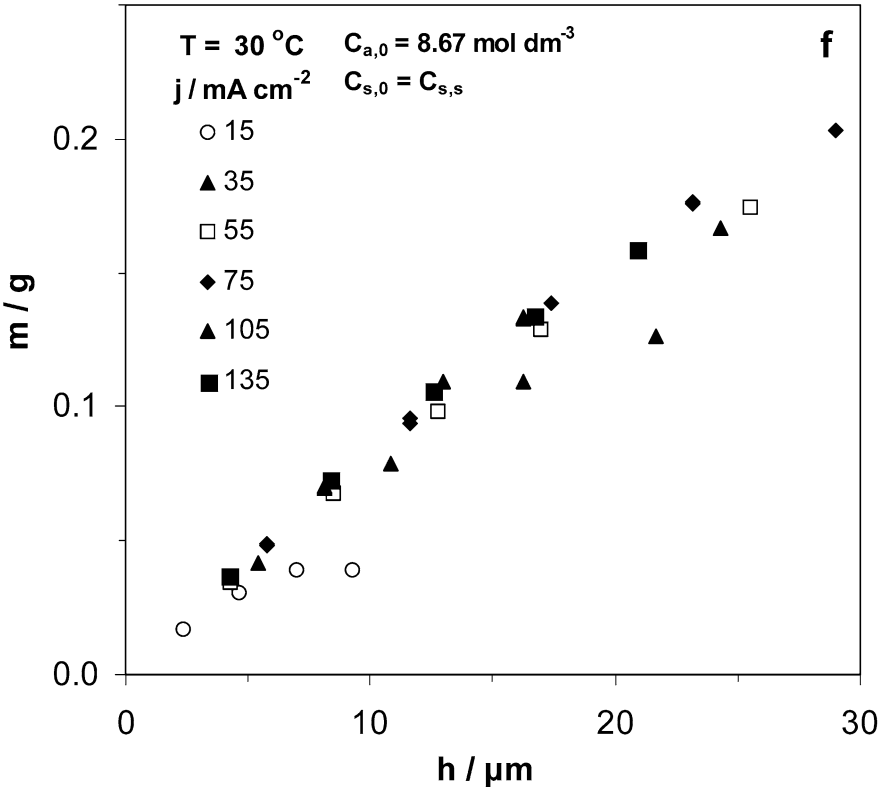
T = 30 °C
$C_{a,0}$ = 8.67 mol dm^{-3}
j / mA cm^{-2}
$C_{s,0}$ = $C_{s,s}$
15
35
55
75
105
135
f
m / g
h / µm
0.0
0.1
0.2
0
10
20
30

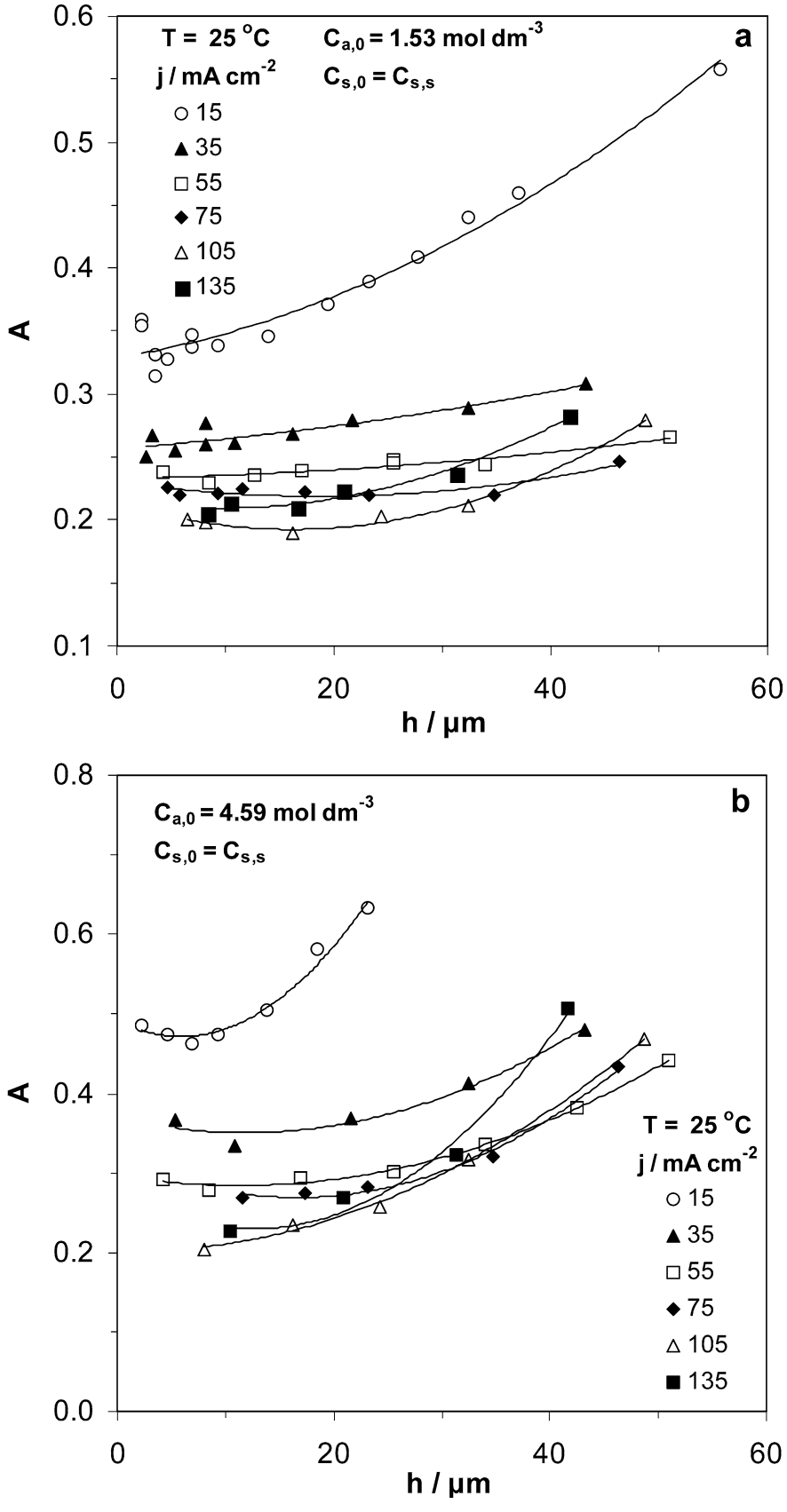

Fig. 6 Variation of the dimensionless factor A with film thickness, $h\{h[t(\Delta V_m) \leq h \leq h(t_m)\}$, at different H_2SO_4 concentrations ($C_{a,0}$), current densities (j), bath temperatures (T), and at saturation $Al_2(SO_4)_3$ concentrations ($C_{s,0} = C_{s,s}$)

Fig. 6 (Contd.)

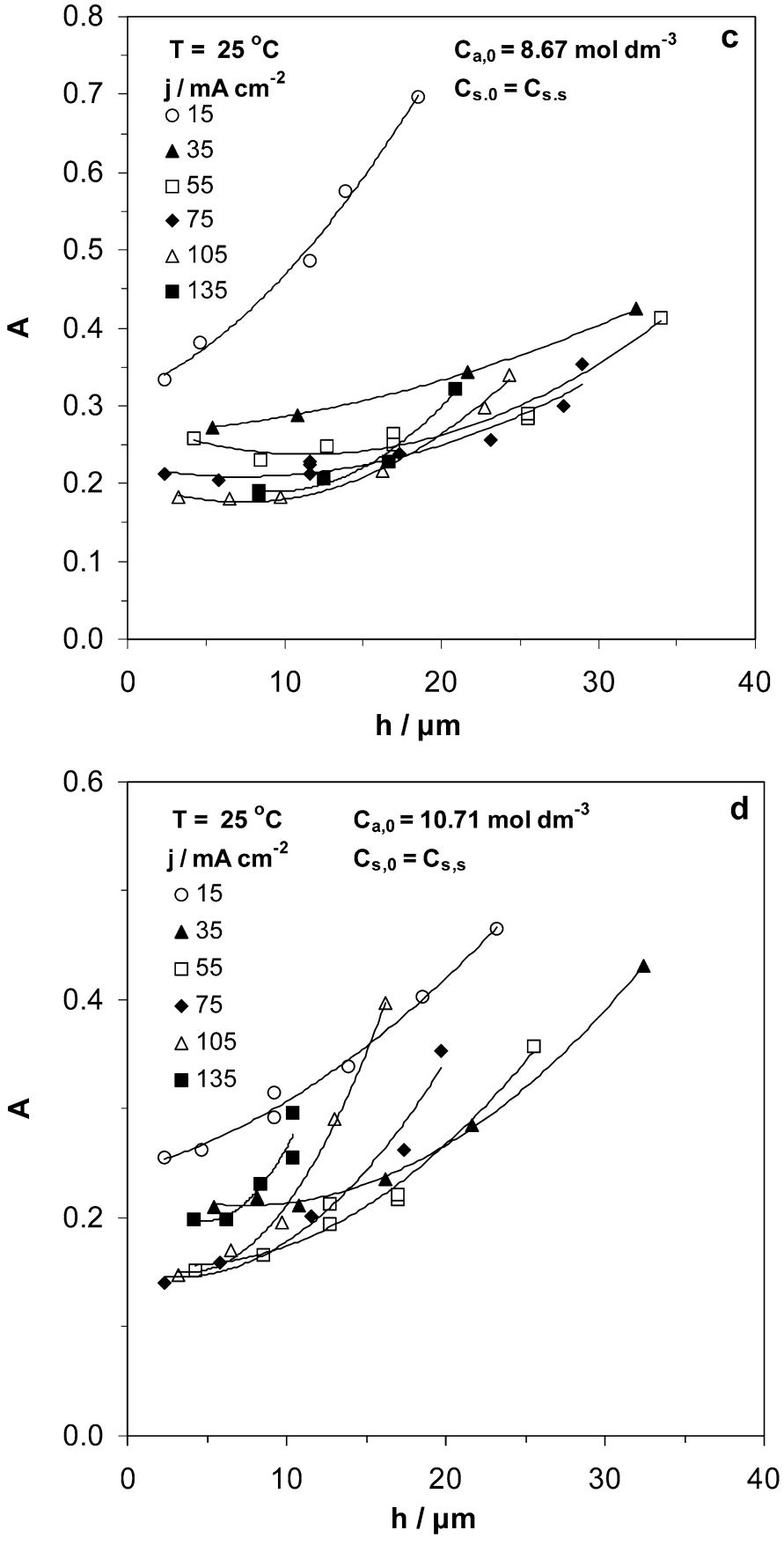
c
T = 25 °C
j / mA cm-2
15
35
55
75
105
135
Ca,0 = 8.67 mol dm-3
Cs.0 = Cs.s
A
h / µm
0.0
0.1
0.2
0.3
0.4
0.5
0.6
0.7
0.8
0
10
20
30
40
d
T = 25 °C
j / mA cm-2
Ca,0 = 10.71 mol dm-3
Cs,0 = Cs,s
A
h / µm
0.0
0.2
0.4
0.6

Fig. 6 (Contd.)

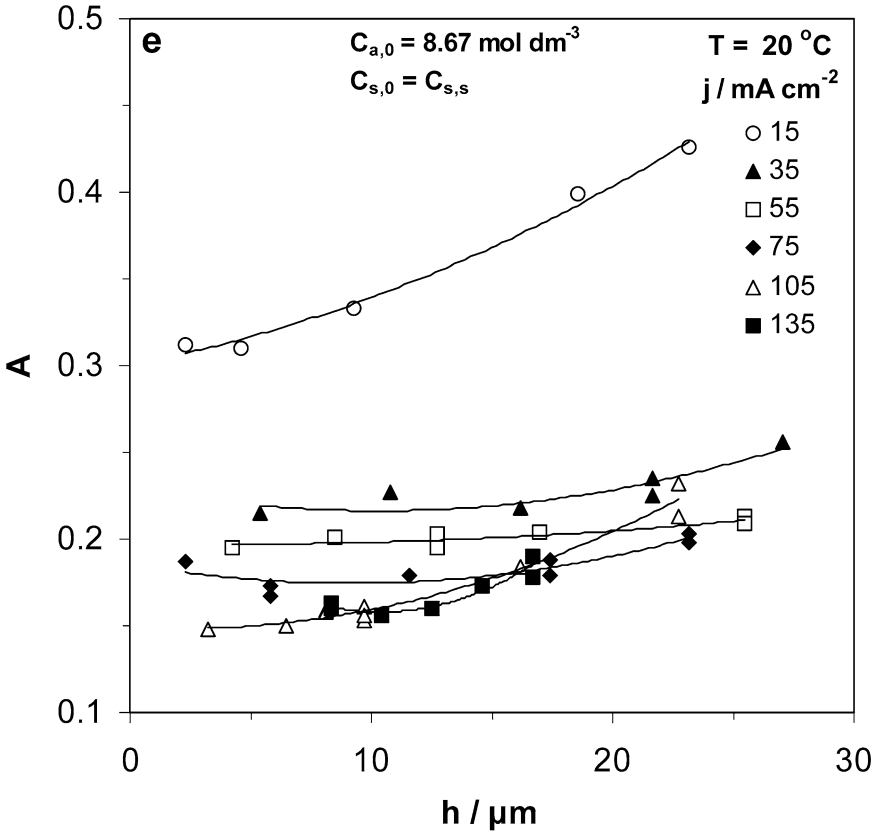
e
$C_{a,0}$ = 8.67 mol dm^{-3}
$C_{s,0}$ = $C_{s,s}$
T = 20 °C
j / mA cm^{-2}
15
35
55
75
105
135
A
h / µm
0.1
0.2
0.3
0.4
0.5
0
10
20
30

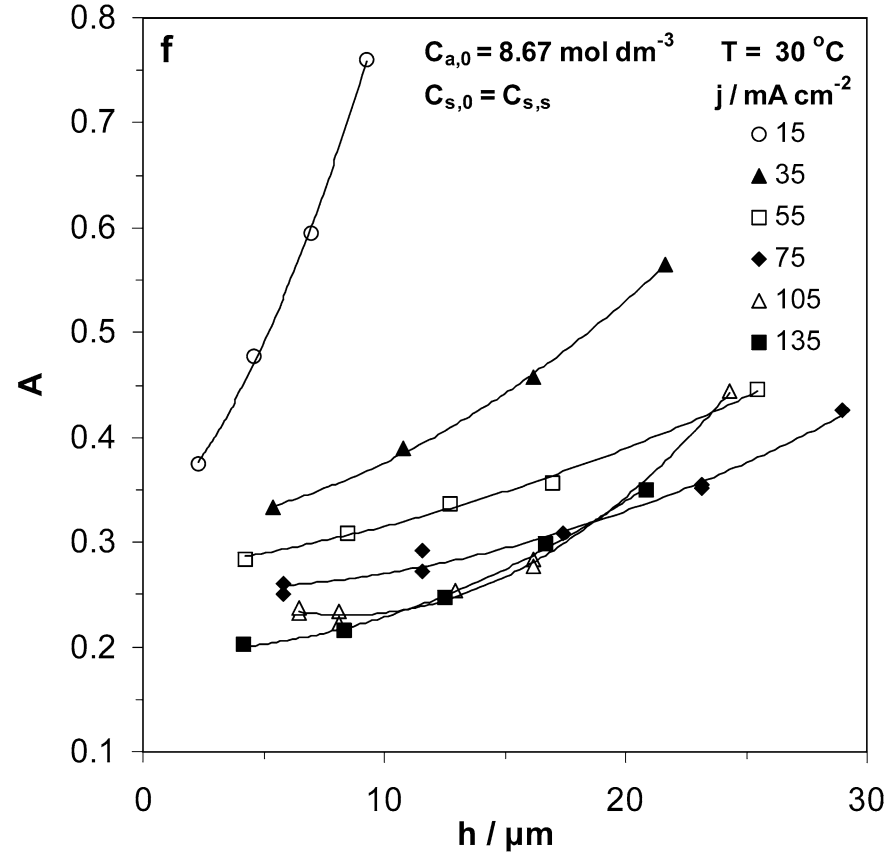
f
$C_{a,0}$ = 8.67 mol dm^{-3}
$C_{s,0}$ = $C_{s,s}$
T = 30 °C
j / mA cm^{-2}
15
35
55
75
105
135
A
h / µm
0.1
0.2
0.3
0.4
0.5
0.6
0.7
0.8
0
10
20
30

Table 1 Values of parameters A_0, A'_1 and A'_2 and of correlation coefficient (COR) derived from fitting Eq. (4) to experimental results

$C_{a,0}$(mol dm^{-3})	T (°C)	j (mA cm^{-2})	$10^4 A_0$	$10^6 A'_1$(μm^{-1})	$10^6 A'_2$ (μm^{-2})	COR^2
1.53	25	15	3,288	1,426	51	0.9622
		35	2,567	660	12	0.8416
		55	2,333	138.2	9.3	0.8774
		75	2,302	−1,220	30	0.8005
		105	2,140	−2,700	100	0.9931
		135	2,157	−1,320	70	0.9745
4.59	25	15	4,914	−6,800	600	0.9773
		35	3,692	−3,200	100	0.9631
		55	2,969	−2,300	100	0.9960
		75	3,198	−6,100	200	0.9909
		105	2,021	−400	100	0.9978
		135	2,838	−8,400	300	0.9851
8.67	25	15	3,149	8,900	600	0.9928
		35	2,632	1,080	120	0.9999
		55	2,821	−7,800	300	0.9691
		75	2,225	−3,700	300	0.9122
		105	2,057	−8,000	500	0.9940
		135	2,762	−18,300	1,000	0.9741
	20	15	3,005	2,600	100	0.9901
		35	2,297	−2,600	100	0.7957
		55	1,976	−250	30	0.7512
		75	1,859	−2,470	130	0.8097
		105	1,492	−740	170	0.9668
		135	2,319	−14,220	680	0.9006
	30	15	3,133	20,400	3,000	0.9994
		35	3,102	2,100	400	0.9987
		55	2,721	2,700	200	0.9945
		75	2,553	−700	200	0.9831
		105	2,898	−14,100	800	0.9955
		135	1,966	−720	390	0.9974
10.71	25	15	2,433	3,900	200	0.9909
		35	2,316	−5,400	400	0.9974
		55	1,608	−2,700	400	0.9722
		75	1,528	−4,500	700	0.9645
		105	1,738	−12,300	1,600	0.9943
		135	2,566	−24,600	2,500	0.8684

Discussion

Composition of pore-filling solution when condensed $Al_2(SO_4)_3$ does not form

$Al_2(SO_4)_3$ is always produced by the so-called field-assisted pore base oxide dissolution [2, 3, 20, 22, 23, 24, 37, 38, 39] and by the purely chemical pore wall oxide dissolution [2, 27, 28, 29, 30, 31] which enters the pore-filling solution, and even in the case $C_{a,0} = 0$ it contains $Al_2(SO_4)_3$ besides H_2SO_4. The mechanism of oxide production in the barrier layer, Fig. 8, predicts that H^+ and Al^{3+} are rejected from the pore base surface in the pore-filling solution at rates J_{H^+} and $J_{Al^{3+}}$ (mol/time) according to the following equations [18]:

$$J_{H^+} = 2^{-1} j S_g F_c^{-1} - 3 j S_g (6F_c)^{-1} D_b^2 D_c^{-2} \quad (5)$$

$$J_{Al^{3+}} = 2^{-1} M_W^{-1} S_g \pi k'' j d_c n D_b^2 = 2 j S_g (6F_c)^{-1} D_b^2 D_c^{-2} \quad (6)$$

$$J_{H^+} \left(J_{Al^{3+}}\right)^{-1} = (3/2)\left(1 - D_b^2 D_c^{-2}\right) D_b^{-2} D_c^2 = (3/2)\left[1 - \left(nD_b^2\right)/\left(nD_c^2\right)\right]\left[\left(nD_c^2\right)/\left(nD_b^2\right)\right] \quad (7)$$

where M_w is the molar mass of oxide, F_c is Faraday's constant and D_c is the cell width which depends only on j and is related to n by $nD_c^2 = 4/3$ [36]. Considering that nD_b^2 varies (from 0.45 to 0.15; i.e. values comparable to the limiting ones met here for $h \to 0$), $J_{H^+}\left(J_{Al^{3+}}\right)^{-1}$ varies from ≈2.3 to ≈11.8.

The transport phenomena inside the pores during anodising in H_2SO_4 and in $H_2SO_4 + Al_2(SO_4)_3$ electrolytes were studied earlier [35, 40] considering regular film growth, constant pore base diameter and temperature along the pores and no formation of condensed $Al_2(SO_4)_3$ for $C_{a,0} \le 1.531$ mol dm^{-3} and $C_{s,0} \le 0.5$ mol dm^{-3}, where the formulation of a relevant system of interlaced differential equations and their solution became possible [35]. Equations embrace J_{H^+} and $J_{Al^{3+}}$ together with a number of other structural, kinetic, etc. parameters.

The dependence of $C_{a,b}$, H_2SO_4 concentration at position x ($C_{a,x}$), $C_{s,b}$ and $Al_2(SO_4)_3$ concentration at position x ($C_{s,x}$) on h, x, j, T, $C_{a,0}$ and $C_{s,0}$ is generally very complex. But at the j values ≤ 35 mA cm^{-2}, the T values and the lower $C_{a,0}$ employed here and $C_{s,0} = 0.5$ mol dm^{-3}, which is lower, but not strongly different, than $C_{s,s} = 0.74$ mol dm^{-3} ($C_{s,0} < C_{s,s}$), their variation is simpler. The $C_{a,x}$ and $C_{s,x}$ values always

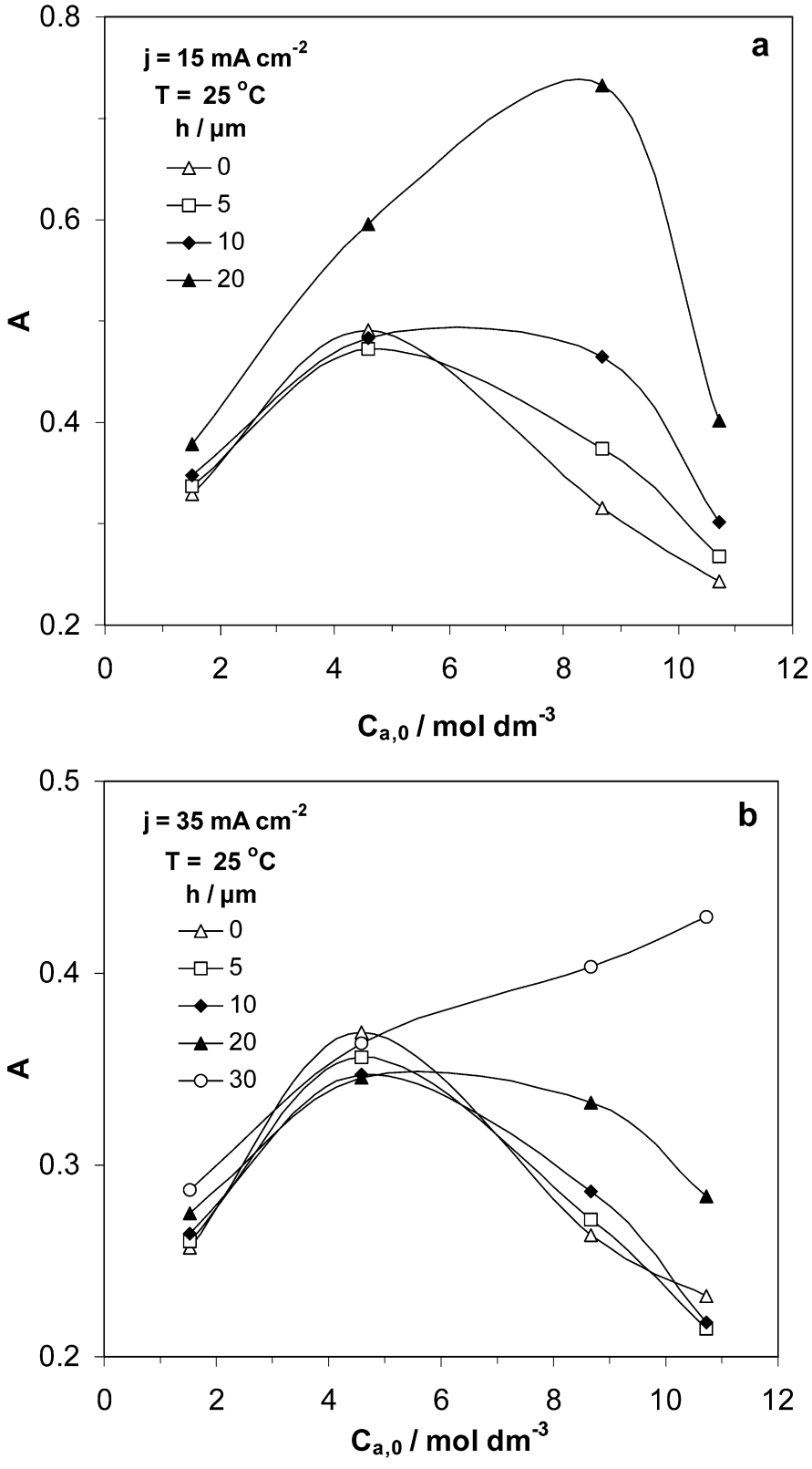

Fig. 7 Variation of the dimensionless factor A with H_2SO_4 concentration ($C_{a,0}$) at different film thicknesses, $h\{h[t(\Delta V_m) \le h \le h(t_m)\}$, and current densities (j) at constant bath temperature $T = 25°C$

increase from the mouths towards the bases of pores and with increasing j and decreasing T [35]. The $C_{s,x} - C_{s,0}$ and $C_{a,x} - C_{a,0}$ values increase with j and decrease with T. Nevertheless, the composition of solution along the pores does not differ appreciably from that of the bath for the abovementioned j values. Thus, H^+ activities in the bath solution ($a_{H^+,0}$), at each position x along the pores ($a_{H^+,x}$) and in the pore bases region ($a_{H^+,b}$) are

Fig. 7 (Contd.)

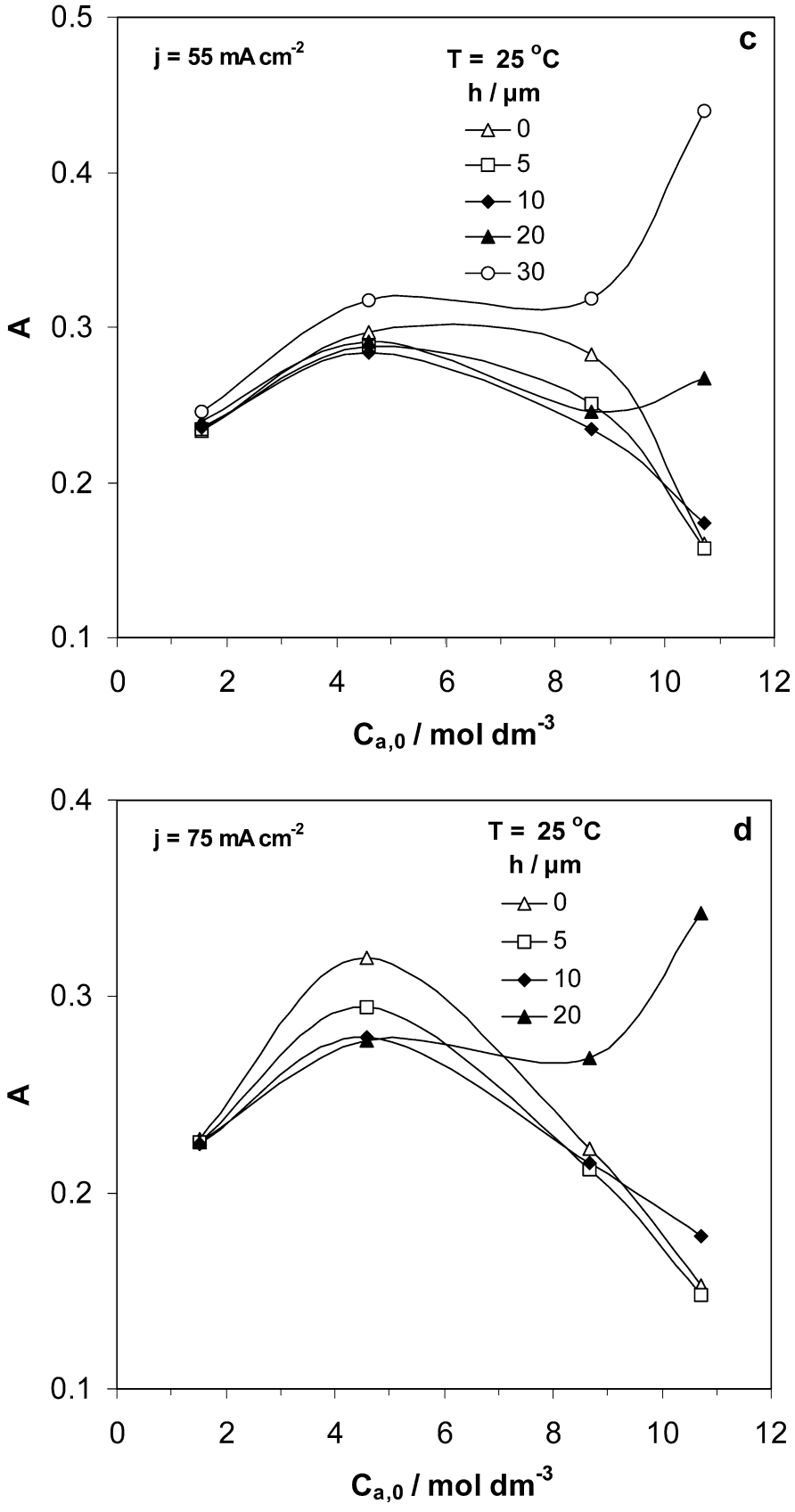
c
j = 55 mA cm-2
T = 25 °C
h / µm
0
5
10
20
30
A
0.5
0.4
0.3
0.2
0.1
0
2
4
6
8
10
12
Ca,0 / mol dm-3
d
j = 75 mA cm-2
T = 25 °C
h / µm
0
5
10
20
A
0.4
0.3
0.2
0.1
0
2
4
6
8
10
12
Ca,0 / mol dm-3

Fig. 7 (Contd.)

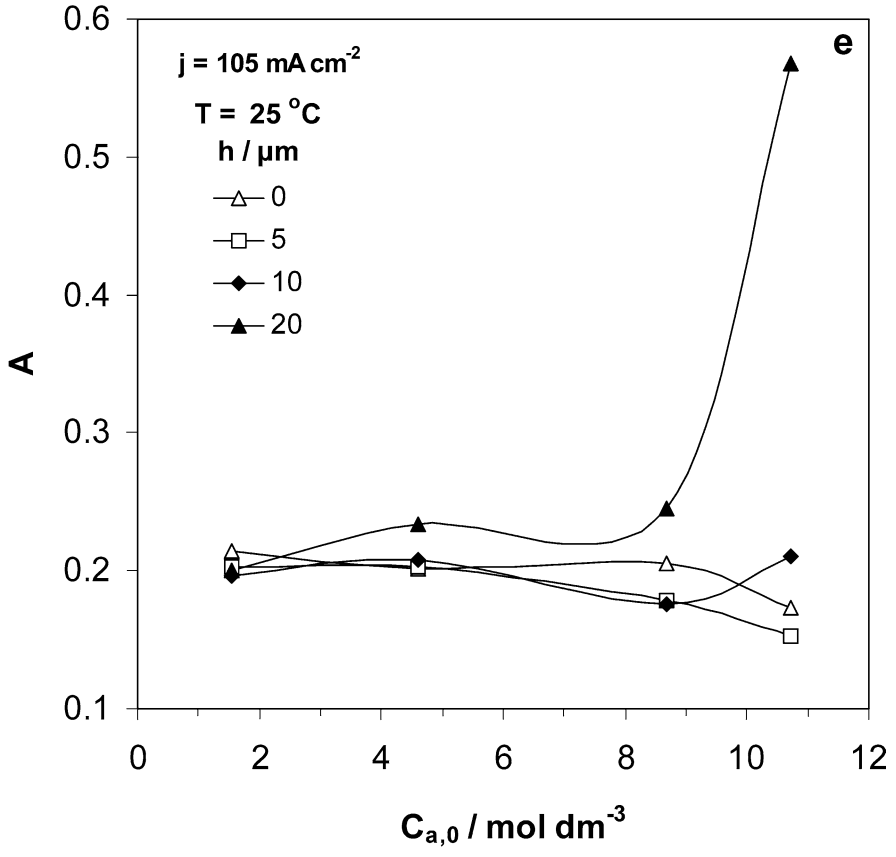
e
j = 105 mA cm-2
T = 25 °C
h / µm
0
5
10
20
A
Ca,0 / mol dm-3

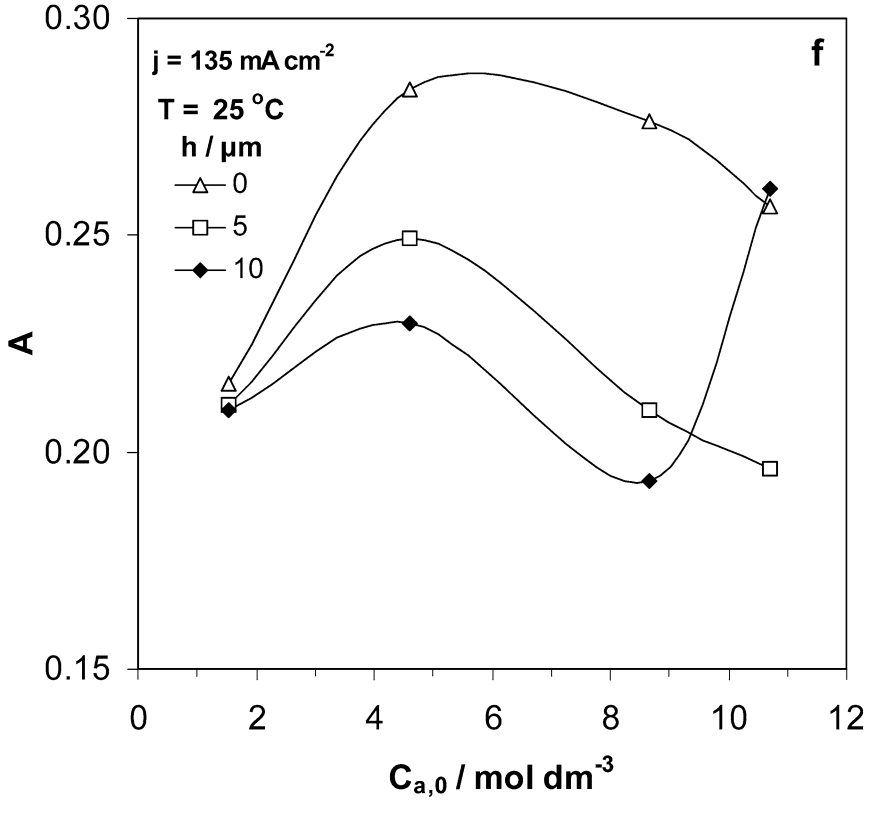
f
j = 135 mA cm-2
T = 25 °C
h / µm
0
5
10
A
Ca,0 / mol dm-3

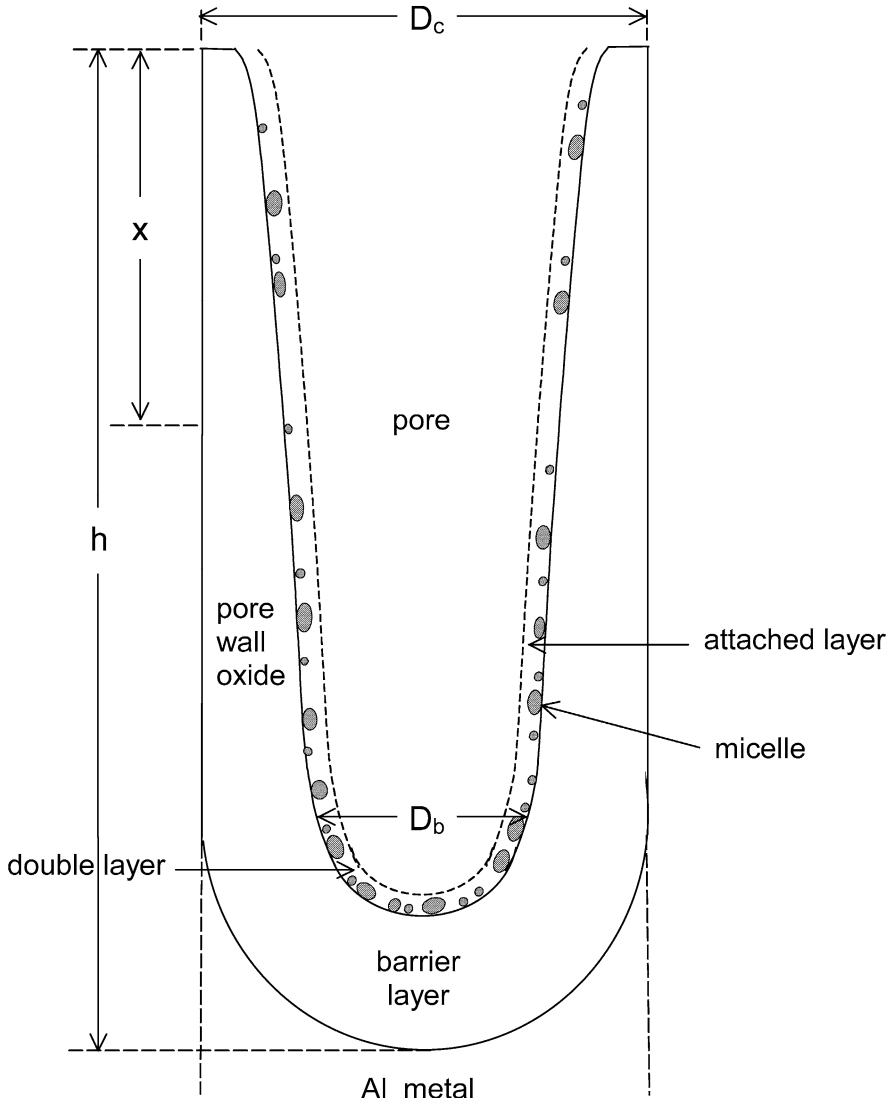

Fig. 8 Schematic representation of the cross section parallel to pore axis of a cell of an anodic alumina film with thickness h where the pore wall oxide, the pore, the barrier layer, the pore base diameter D_b, the cell width D_c, the double layer on pore base surface and the attached layer on the pore wall surface where the formation of interface colloidal $Al_2(SO_4)_3$ nanoparticle micelles takes place are distinguished

also close each to other. But as shown for $C_{a,0} = 15\%$ w/v and $C_{s,0} = 0$ [40] appreciable variations of $C_{a,x}$ and $C_{s,x}$ along the pores appear at higher j values which is expected to be valid also for $C_{s,0} > 0$. In denser solutions and $C_{s,0} > 0$, when condensed $Al_2(SO_4)_3$ does not form, $C_{a,x}$ and $C_{s,x}$ are also expected to increase with x more strongly at higher j values and accordingly $a_{H^+,x}$ varies.

Composition of pore-filling solution at $C_{s,0} = C_{s,s}$

In this case it is expected that at each T any decrease of nD_b^2 for any reason will cause an increase of $J_{H^+}\left(J_{Al^{3+}}\right)^{-1}$ which, in turn, is expected to yield a tendency for a rise of the $C_{a,b}/C_{s,b}$ value. When condensed $Al_2(SO_4)_3$ forms there is also a tendency for $C_{a,x}$ and $C_{s,x}$ to increase towards the pore bases. For $C_{a,0} < C_{a,0,m}$ irrespective of the $J_{H^+}\left(J_{Al^{3+}}\right)^{-1}$ value, because $C_{s,s}$ decreases with $C_{a,0}$ at $C_{s,0} = C_{s,s}$, precipitate should be formed inside the pores. But if it were really formed, the process should cease early, which is not the case. Then, the solution inside the pores must become unsaturated or supersaturated. Due to the above increase of $C_{a,x}$ and $C_{s,x}$ towards the pore bases the solution must be supersaturated and its composition is shifted above the $C_{s,s}$ vs. $C_{a,0}$ curve, Fig. 1.

Thus, the supersaturation $C_{s,x} - C_{s,0}$ increases towards the pore bases. The supersaturation and catalytic action of both the field at pore bases and all the solid surface of pore walls result in the formation of micelles [25] which consumes $Al_2(SO_4)_3$ and locally lowers $C_{s,x}$. The surface concentration of micelles [25] must increase towards the bases of pores. Because $C_{s,x}$ and $C_{a,x}$ together tend to increase with x and for $C_{a,0} < C_{a,0,m}$ the $C_{s,s}$ (and $C_{s,x}$) value decreases with $C_{a,0}$, irrespective of $J_{H^+}\left(J_{Al^{3+}}\right)^{-1}$ value, the formation of micelles at each x position regulates the composition to be close to the solubility curve, Fig. 1, and at its corresponding $C_{s,s}$ vs. $C_{a,0}$ point.

For $C_{a,0} > C_{a,0,m}$ the above are valid probably when j and therefore $J_{H^+}\left(J_{Al^{3+}}\right)^{-1}$ are adequately low. But

under some conditions (i.e. not low enough j values), because $J_{H^+}\left(J_{Al^{3+}}\right)^{-1}$ may be not adequately low, some trend for a shift of composition on the right and down the solubility curve may occur. In this case although $C_{a,x} > C_{a,0}$ and $C_{s,x} > C_{s,0}$, the solution inside the pores becomes unsaturated. Thus, only in this case the pore-filling solution is unsaturated and not at lower $C_{s,0}$ values as assumed earlier [25].

From data published earlier [18] for $C_{s,0} = 0$ and $T = 25°C$ at $C_{a,0} = 15$, 25 and 45% w/v, $a_{H^+,0} = 0.52$, 0.83 and 1.50 mol dm^{-3}. From the ratios of $a_{H^+,0}$ at 65, 85 and 105% w/v to that at 15% w/v [41], $a_{H^+,0}$ is found to be $\approx$1.89, 2.17 and 1.63 mol dm^{-3} at these $C_{a,0}$ values. Hence $a_{H^+,0}$ exhibits a maximum around $C_{a,0} = C_{a,0,m} = 95\%$ w/v which must be higher than 2.17 mol dm^{-3}. The addition of $Al_2(SO_4)_3$ in the bath at $C_{a.0} \geq 15\%$ w/v increases $a_{H^+,0}$. For example at $C_{a.0} = 15\%$ w/v and $C_{s,0} = 0.34$ and 0.75 mol dm^{-3} $a_{H^+,0}$ was $\approx$19 and 42% respectively higher than that at $C_{s,0} = 0$ [18]. In the cases of $C_{a,0} = 45$, 85 and 105% w/v, the $C_{s,s}$ values are insignificant compared to $C_{a,0}$ values. Hence $a_{H^+,0}$ values must differ only slightly from those at $C_{s,0} = 0$ and there is no need for their determination which, in addition, is complex enough and beyond the scope of this study. Thus at $C_{s,0} = C_{s,s}$ $a_{H^+,0}$ also passes through a maximum at $C_{a,0} \approx C_{a,0,m}$ but the differences for the various $C_{a,0}$ values are lower than those at $C_{s,0} = 0$.

From the above discussion it is inferred that, due to the regulating mechanism imposed by the saturated bath, for the $C_{a,0}$ values $< C_{a,0,m}$ used, $C_{a,0} < C_{a,b} < C_{a,0,m}$ and $a_{H^+,0} < a_{H^+,b} < a_{H^+,m}$, while for $C_{a,0} > C_{a,0,m}$ and the $C_{a,0}$ used $C_{a,0,m} < C_{a,0} < C_{a,b}$ and $a_{H^+,m} > a_{H^+,0} > a_{H^+,b}$. As noted the $C_{a,b} - C_{a,0}$ and $a_{H^+,b} - a_{H^+,0}$ values become appreciable at high j values. The $C_{a,0}$ values around $C_{a,0,m}$ were chosen to differ appreciably from $C_{a,0,m}$ and the above order of $C_{a,0}$, $C_{a,b}$ and $C_{a,0,m}$ and of $a_{H^+,0}$, $a_{H^+,b}$ and $a_{H^+,m}$ be thus valid for all t, h and j values, not only for $C_{a,0} > C_{a,0,m}$, but for all $C_{a,0}$ values $< C_{a,0,m}$ examined as well and the agitated baths employed. This facilitates the analysis, since the change of this order renders it complex enough [41].

Establishment of a temperature gradient along the pores and its effect on the composition of pore-filling solution

The heat evolved during anodic oxidation of Al mainly in the pore bases region, which increases with j, is dissipated to the bath solution mainly through the pore-filling solution, which has higher thermal conductivity than the solid pore wall oxide. As shown [32] a gradient of T is set up along the pores. This increases with decreasing T due to an expected small decrease of thermal conductivity of solution, supposed to behave similarly to H_2O [42], and mainly to the decrease of the average value of cross sectional surface area of pores per unit of specimen surface through which the heat is transferred, and with increasing j, due to the aforementioned reason together with the increasing rate of evolved heat. The density (or viscosity) of solution, which as verified increases with $C_{a,0}$, may exert a positive effect on it. The temperature around pore bases T_a (anodising temperature) thus becomes higher than T and that along the pores T_x decreases towards the pore mouths while $T_x - T$ increases with decreasing T [32] and increasing x and j and probably with $C_{a,0}$.

Since solubility increases slightly with T, Fig. 1, and $T_x > T$, the $C_{a,x}$, $C_{s,x}$ and $C_{s,x} - C_{s,s}$ decrease to some extent compared to those corresponding to each T. Thus the composition of pore-filling solution changes somewhat compared to that described previously, which perhaps should be taken into consideration for an accurate/complete interpretation of results. As will be seen later, the rise of temperature inside pores significantly affects the whole mechanism of film growth mainly at high j values.

Parameters affecting D_b and the surface fractions occupied by micelles

As shown earlier [18], D_b and D_c obey the following general equations:

$$\left(1-\theta_b\right)^{-1}\left[\left(nD_b^2\right)^{-1}-\left(nD_c^2\right)^{-1}\right]=j^{-1}\pi B_1\left\{\exp\left[-\Delta H^0 - W_1N+\left(2n_1a_1'+n_1a_1\right)F_cE_b/\left(RT_a\right)\right]\right\}\left(k_W a_{H^+,b}^{-1}+b\right) \tag{8}$$

$$\left[\left(1-\theta_b\right)nD_c^2\right]^{-1}=2^{-1}j^{-1}\pi B_2\exp\left[\left(-W_2N + n_2a_2F_cE_b\right)/\left(RT_a\right)/\left(RT_a\right)\right] \tag{9}$$

$$\left(nD_b^2\right)^{-1}\left(nD_c^2\right)=1+2B_1B_2^{-1}\left\{\exp\left[\left(-\Delta H^0-W_1Nc+W_2N + \left(2n_1a_1'+n_1a_1-n_2a_2\right)F_cE_b\right)\left(RT_a\right)\right]\right\}\left(k_W a_{H^+,b}^{-1}+b\right) \tag{10}$$

where θ_b is the pore base surface fraction occupied by micelles; B_1 and B_2 are constants; ΔH^0 is the standard enthalpy of reaction $Al^{3+}_{(\text{bare sites})} + OH^-_{(b/d)} \rightleftharpoons Al^{3+}OH^-$ on that surface, where the subscript b/d means the barrier layer/double layer interface; W_1 and W_2 are the activation energies for OH^- and O^{2-} migrations; n_1 and n_2 are the valences of OH^- and O^{2-}; a_1 and a_2 are the half-jump (activation) distances inside the barrier layer; a'_1 is that distance of OH^- transfer from the surface of double layer to a coordinated site of oxide surface; N is the Avogadro constant; R is the universal gas constant; E_b is the field strength on the pore base surface; k_w is the ionic product of H_2O; b is a parameter increasing with E_b and decreasing with T_a. The $-W_1N + n_1a_1F_cE_b$ and $-W_2N + n_2a_2F_cE_b$ values are < 0. When micelles do not form $\theta_b = 0$ and at each j value, D_b remains constant during anodising and depends only on T_a and $a_{H^+,b}$.

These equations show that at constant T_a and j, E_b depends only on θ_b and increases with it. D_b depends only on $a_{H^+,b}$ and E_b (or θ_b), increasing with the first and decreasing with the second. Also, E_b increases with j. Equation 9 shows that as T_a increases θ_b decreases. This is consistent with the fact that the rise of T_a disfavours the development of micelles and favours their dissolution [25].

The formation of micelles at pore bases under supersaturation conditions is thus favoured by the increase of $C_{s,b}-C_{s,0}$, E_b and j and decrease of T_b. Results are consistent with the fact that their formation is favoured by increasing concentration (or activity) of Al^{3+} and SO_4^{2-}. The concentration of Al^{3+} coming from $Al_2(SO_4)_3$ becomes minimum at $C_{s,0}=C_{s,s,m}$ while that of all SO_4^{2-} coming from both $Al_2(SO_4)_3$ and H_2SO_4, with second dissociation constant $k_2=1.2\times10^{-2}$ at 25°C [43], becomes minimum at a $C_{s,0}$ slightly lower than $C_{s,s,m}$. Thus the formation of micelles is less favoured at a $C_{a,0}$ between that and $C_{a,0,m}$, i.e. slightly lower than $C_{a,0,m}$ or roughly $\approx C_{a,0,m}$. Probably it is affected by the purity of pore base surface and density (or viscosity) of solution reinforcing it (secondary factors). Thus, θ_b increases mainly with E_b, j, $C_{s,b}-C_{s,s}$ and $C_{s,s}$ and decreases with T_b. It increases also with h, since $C_{s,b}-C_{s,s}$ varies similarly. At constant E_b, j, $C_{s,b}-C_{s,s}$ and h, $C_{s,b}$ will pass through a minimum around $C_{a,b}\approx C_{a,0,m}$, thus θ_b passes through a minimum around $C_{a,b}\approx 95\%$ w/v or roughly around $C_{a,0}\approx 95\%$ w/v.

The rate of pore wall dissolution reaction at a position x (r_x/length time^{-1}) depends linearly on the local reaction rate constant ($k_{d,x}$), which increases with increasing T_x and decreasing local concentration of incorporated electrolyte anions in a thin surface layer on pore walls [18, 19], the activity a_{H^+} in the pore-filling solution at a site neighbouring to the previous one, $a_{H^+,x}$, and the local free surface fraction not occupied by micelles $(1-\theta_x)$ [25]

$$r_x = k_{d,x} a_{H^+,x}(1-\theta_x). \tag{11}$$

Micelles formation seems to be enhanced towards the pore bases irrespective of anion concentration variations under supersaturation conditions. Thus θ_x increases with $C_{s,x}-C_{s,0}$, and therefore with x, and with $C_{s,x}$ and thus at constant $C_{s,x}-C_{s,0}$ and x it passes through a minimum at $C_{s,x}\approx C_{s,s,m}$ or roughly at $C_{a,0}\approx C_{a,0,m}$. Also it increases with decreasing T_x or T.

The above-described variation of θ_b and θ_x with different parameters is significant since it can reveal the critical role of micelles in the whole mechanism of oxide growth as shown in the following sections.

Dependence of the mechanism of oxide growth on pore shape

As earlier shown [33, 41], when pore diameter increases from the base to the mouths of pores, a case is met when r_x is lower than that around the pore mouths ($r_{x=0}$), $r_x \le r_{x=0}$, i.e. the pore shape is that of an elongated cone, trumpet or half barrel, etc., the m or h, in cases of uniform film thickness, or the average h (h_a), in cases of non-uniform thickness, vs. t plots present a (like) breaking point around $t=t_m$ more or less clearly. If pores were strictly cylindrical these plot profiles would coincide. But since pore wall dissolution always occurs along the pores, the m vs. t plots differ slightly from those of h vs. t; thus at $t \le t_m$ or t_l, the first always bend to the right while the second are linear. But other strong trends and details, like breaking points etc., remain identical for both plots.

Under specific conditions the pores acquire a shape like that of an amphora [41] for $t > t_m$; beyond the pore base a maximum diameter, a neck and finally the pore mouth diameter comparable to D_c successively appear. This case is met when at $t>0$, for some reasons r_x in a region along the pore length or along the whole pore length becomes $> r_{x=0}$. In this case, besides t_m, another time t_m' is distinguished, at which this maximum pore diameter behind the pore mouths approaches first the cell width. The m or h (or h_a) vs. t plots present (like) breaking points around $t=t_m$ and t_m and then an inflection point, or successively a maximum, a minimum and an inflection point, after which an increase is observed. For $t > t_m'$ oxide starts to cut off from the film in the form of very thin transparent scales, clearly observed in the non-stirred bath [44], which are removed, at a rate initially accelerated, as the phenomenon is gradually spread over a larger surface area, and then retarded. When the maximum diameter lies close to pore mouths an inflection point only appears, but when it lies at a significant distance a maximum and a minimum successively appear followed by an inflection point around which the cut and removal of material, or the detachment of the external film layer, end.

The plot profile in the second case is explained by the fact that the rate of m or h_a increase due to the oxide production in the barrier layer region [32] is higher than that of their decrease between the second breaking point and maximum. After that a reverse trend is established up to the minimum after which the trend is again reversed up to the last inflection point. In the first case the rate of increase of m or h_a is higher than that of their decrease at all t values, while they may be balanced around the inflection point. Since a quasi-steady-state exists inside pores, a decrease of h_a returns the distribution of electrolyte composition along the pores to a situation similar to that corresponding to a comparable h_a at a lower t.

Interpretation of the variations of D_b, nD_b^2 and ΔV with j, T and $C_{a,0}$ ($h \to 0$) and with h, j, T and $C_{a,0}$ ($h>0$): critical role of micelles appearing on the pore base surface in the film growth mechanism

When $h \to 0$, $a_{H^+,x}\approx a_{H^+,b}\approx a_{H^+,0}$ and $\theta_x \approx \theta_b$. Since n (and therefore D_c) depend only on j, as shown in Eqs. (8), (9)

and (10), at each j, both nD_b^2 and D_b vary so that they tend to pass through a maximum around $C_{a,0,m}$ affected by $a_{H^+,b}$, and through a minimum around $C_{a,0,m}$ affected by θ_b. These opposing effects must be roughly comparable but the first is slightly higher and their combined result yields a maximum at a $C_{a,0}$ different than $C_{a,0,m}$, i.e. in the region extending from 45% up to 85% w/v, as shown in Fig. 7 and Table 1.

The local field strength across the barrier layer increases from the pore base surface to the metal/oxide interface [18]. Hence at each j, considering constant field strength in the vicinity of metal/oxide interface, the potential drop across the barrier layer increases with E_b, and therefore with θ_b, and with the thickness of barrier layer $2^{-1}(D_c - D_b)$, and therefore with decreasing D_b. It is always close to ΔV [18, 36]. When $h \rightarrow 0$ and at each j, ΔV must pass through a minimum at $C_{a,0} \approx 45\%$ w/v affected by D_b and through a minimum at $C_{a,0} \approx C_{a,0,m}$ affected by θ_b. Their combined result can then yield two distinct minima of ΔV around $C_{a,0} = 45\%$ w/v and $C_{a,0,m}$ separated by a small maximum or roughly a large well-like minimum with a plateau at its depth between these two $C_{a,0}$ values. The lower ΔV values for $h \rightarrow 0$ (e.g. ΔV_m values) predicted in the region from $C_{a,0} \approx 45\%$ w/v to $\approx C_{a,0,m}$, Figs. 2 and 3, are thus explained.

At each $C_{a,0}$, the effect of j, T_a and θ_b on D_b, Eqs. (8), (9) and (10), the decrease of n with j [26], the fact that $T_a - T$ increases with increasing h and j and decreasing T and probably with the density of bath (or $C_{a,0}$) and the effect of T_a on $C_{s,b}$ and $C_{a,b}$, which lie close to the solubility curve under supersaturation conditions and depend on T, j, h and $C_{a,0}$ in a complex manner, can generally justify the variation of D_b and nD_b^2 with h, T and j; for example D_b decreases with h and increases with T and seems not largely affected by j, since the increase of j raises T_a and θ_b, which oppositely affect D_b.

Because at each t or h a (quasi) steady state dominates inside the pores, the increase of θ_b and decrease of D_b keep in pace with the increase of h. Since the variation of ΔV during the film growth reflects primarily the variations of D_b and θ_b, from their variations with h it is easily inferred that ΔV increases with h or the ΔV vs. t plots are qualitatively similar to those of m and h or h_a vs. t plots.

At $C_{a,0} = 105\%$ w/v $> C_{a,0,m}$ and $h > 0$, considering that $\theta_b = 0$ and $\theta_x = 0$, the distribution of $a_{H^+,x}$ predicts a trumpet pore shape [41]. It seems that $J_{H^+}\left(J_{Al^{3+}}\right)^{-1}$ is not adequately low and the composition of solution inside the pores is shifted gradually with t or h (or h_a) below the solubility curve slightly at low j values and significantly at high j values. This shift exerts a slight only effect on θ_b due to the strong increase of Al^{3+} and anion concentrations across the double layer towards the pore base surface [25]. But it exerts a significant effect on θ_x which is high around the pore mouths ($x = 0$), as a result of saturated bath solution in their vicinity, and near pore bases ($x \rightarrow h$), where necessarily $\theta_x \rightarrow \theta_b$, and is lower at intermediate x positions where the composition is shifted below the solubility curve.

Thus at $t > t_m$, θ_x happens to become minimum in a region along the pores around which, irrespective of the $a_{H^+,x}$ and T_x distributions, $k_{d,x}$ becomes maximum which, in time, yields a maximum pore diameter at a position which, as expected, lies inside the previous region. The positions of minimum θ_x and of maximum diameter are shifted more towards pore bases as h and j increase, since θ_b, although increasing with h and j, is shifted more below the θ_b values corresponding to solubility curve as a result of rising $J_{H^+}\left(J_{Al^{3+}}\right)^{-1}$ with both h and j due to the decrease of nD_b^2, Eq. (7). The aforementioned mechanism of film growth and the anticipated m and h or h_a vs. t plots explain the ΔV vs. t or h plots. A detailed examination of the m and h_a vs. t plots must show a similar behaviour. A similar pore shape can occur even at other $C_{a,0}$ values and different j values at high enough t or h values. The main reasons for that are probably the decrease of D_b with h (or h_a) and the gradual closure of pores together with an increase of T_x towards the pore base region yielding together with the decrease of θ_x towards the pore mouths a maximum diameter at high enough t or h values at a position behind, but rather near, pore mouths around which $r_x > r_{x=0}$. The maximum in the ΔV vs. t plot at $C_{a,0} = 45\%$ w/v and the lower j is thus explained.

Despite this variation of θ_b with h and j at $C_{a,0} = 105\%$ w/v it can be appreciably higher than at other $C_{a,0}$ values, like 85% w/v, at the lower j, since for example the concentrations of Al^{3+} and SO_4^{2-} in the double layer are also higher taking into consideration that at this j value the composition of electrolyte inside the pores remains still close to the solubility curve. This together with the lower D_b for $h \rightarrow 0$ at $C_{a,0} = 105\%$ w/v than at the other $C_{a,0}$ values and the variation of θ_b and D_b with h justify the on average higher rate of increase of ΔV with t or h at this j than at the other $C_{a,0}$ values. But at higher j values the appreciable removal of that composition from the solubility curve acts oppositely so that the average rate of ΔV increase with t or h generally does not differ strongly from that at the remaining $C_{a,0}$ values and in the corresponding t or h regions of ΔV increase.

Generally, the dependence of ΔV on h, j, T and $C_{a,0}$ is explained by their effect mainly on D_b, θ_b and T_a. Although the results of ΔV and A (or p) are commented for $h \le h(t_m)$ at different $C_{a,0}$ values and j values, those of ΔV at $C_{a,0} = 105\%$ w/v and at $C_{a,0} = 45\%$ w/v and the lower j value were also commented for $h > h(t_m)$, as they confirm the cited theory. The above discussion highlights the critical role of micelles appearing on the pore base surface in the film growth mechanism.

Interpretation of the effect of $C_{a,0}$, h, j and T on A and of the relative positions of A vs. h plots at different j values: critical role of micelles appearing on both the pore base and wall surfaces in the film growth mechanism

The effect of j, T, h and $C_{a,0}$ on n, T_a, D_b, $C_{a,b}$, $C_{s,b}$, and therefore on θ_b, as well as on T_x, $C_{a,x}$, $C_{s,x}$ and θ_x and

their relevant effects on r_x and the average along the pores r_x were previously described. The θ_b and θ_x are generally high enough under supersaturation conditions affecting D_b and r_x; D_b decreases with h and r_x is generally low enough but increases with T_x; also θ_x decreases, and r_x rises, as the electrolyte composition inside pores beyond their mouths is shifted below the solubility curve under non-saturation conditions, $C_{a,0} > C_{a,m}$, more as both h and j increase. Their effect on A justifies the A vs. h plot profiles, Fig. 6, as well as those of Fig. 7.

Their effect also justifies the relative positions of A vs. h plots at different j values, Fig. 6. Under supersaturation conditions, as j increases the effect of increasing θ_b on D_b ($h \to 0$) predominates over that of increasing T_a on D_b up to ≈105 mA cm^{-2} at the lower T values or up to a value ≥135 mA cm^{-2} at the higher T. But the effect of increasing average θ_x on r_x predominates over that of increasing average T_x along the pores only up to ≈75 mA cm^{-2} at $C_{a,0} \leq 85\%$ w/v. At higher j values the effect of increasing T_a and the average T_x with j predominates over that of θ_b and θ_x variations with j and the trends for plots shift are reversed. In other words the increase of j enhances the formation of micelles reinforcing the control of oxide growth up to the aforementioned j limits beyond which the concomitant excessive rise of T_a and T_x exerts an opposite effect. At $C_{a,0} = 105\%$ w/v both j limits are appreciably lower, since as h and j increase, the electrolyte composition inside pores is shifted below the solubility curve and, in addition to the rise of T_x with j, the average θ_x increases with j at a rate lower than previously or even starts to decrease with j beyond some j value. The fact that the first j limit is also lower is due to the fact that A_0 is derived from the treatment of experimental results concerning $h > 0$ which embody such influences.

As previously mentioned T exerts a negative effect on the appearance and development of micelles. As a result of the latter and of the positive effect of T on D_b, Eq. (8), and on $k_{d,x}$, as also noted earlier, both D_b and A (or p) generally increase with T as is indeed observed in Fig. 6c, e and f. The above discussion also highlights the critical role of micelles formed on both the pore base and wall surfaces in the film growth mechanism.

Interpretation of earlier results: optimisation of the conditions for obtaining regularly grown films with desired porosity

Earlier [33] it was shown that at $C_{s,0} = 0$, $j = 15$ mA cm^{-2} and $C_{a,0} = 15$–105% w/v, A_0 also exhibits a maximum at around $C_{a,0} = 45\%$ w/v, while at each $h > 0$, A exhibits a maximum at 45% w/v $< C_{a,0} < 65\%$ w/v shifted towards higher $C_{a,0}$ values as h increases. This behaviour is qualitatively similar to that found here. This variation of A_0 or A may be due to the fact that during anodising, micelles can also start to form at least in the pore base region at $C_{s,0} = 0$ and 45% w/v $< C_{a,0} < 65\%$ w/v; otherwise the maximum should appear at $C_{a,0} \approx 95\%$ w/v. The formation of micelles from these relatively low $C_{a,0}$ values shows that (i) the increase of $C_{a,0}$ (or of density/viscosity of solution) enhances the increase of $C_{a,x}$, $C_{s,x}$, $C_{a,b}$ and $C_{s,b}$ so that $C_{a,b} - C_{a,0}$ and $C_{s,b} - C_{s,0}$ generally become significant and/or (ii) the Al^{3+} and SO_4^{2-} concentrations in the double layer on the pore base surface, which probably becomes thicker as the density of solution increases, increase strongly [25] from the pore-filling solution to the surface, much more than along pores beyond this layer; the variation of concentrations in (ii) seems much more significant. A qualitatively similar relevant variation of ions concentrations may also occur in the attached layer on the pore wall surface. Nevertheless, appreciable differences are generally observed in the values of A_0 and A at different h values found here from those at $C_{s,0} = 0$ [33], as expected.

At $C_{s,0} = 0$, $j = 15$ mA cm^{-2} and $C_{a,0} = 85\%$ w/v a similar behaviour as regards the ΔV, m and h (or h_a) vs. t plots [41] to that found here at $C_{a,0} = 105\%$ w/v and the higher j values was also observed which was explained by the fact that $a_{H^+,x}$ becomes maximum $\left(a_{H^+,m}\right)$ at a position inside pores and a relevant complex analysis. But as concluded here micelles must form around pore bases and probably exist along some length of pores from the bases to the mouths of pores. After their formation in the pore base surface they may remain attached on pore walls where they are driven by the mechanism of oxide production and growth of porous layer around the pore bases region [3, 18, 32, 36, 40, 45] until their subsequent detachment along this length and dissolution. Thus the change of θ_x, associated with that the electrolyte composition inside pores lies down the solubility curve, along the length of pores where micelles exist must also be taken into consideration for offering a complete explanation.

The present and earlier results [25, 34, 35] show that pitting is disfavoured as θ_b, T and $a_{H^+,0}$ rise. The θ_b and $a_{H^+,0}$ pass through a minimum and maximum respectively near $C_{a,0,m}$. Their effects seem comparable at low $C_{a,0}$ values, thus the j limit is neighbouring for $C_{a,0} = 15$ and 45% w/v. The observed more intense pitting at $C_{a,0} = 45\%$ w/v above that j limit is due to the fact that although the acidity is higher favouring regular growth, θ_b is much lower and the effect of micelles on film growth mechanism is much less effective. At higher $C_{a,0}$ values, although their combined effect on the j limit is unknown, it exceeds 135 mA cm^{-2}.

Figures 6a–d and 7a–d reveal the ability to optimise the production of desired high- or low-p regularly grown films at constant T. This is valid also for the real surface, since it increases with p and n [11]. From Figs. 6c, e and f concerning $C_{a,0} = 85\%$ w/v it seems that the decrease of T further reduces p at each h, while, as already mentioned, films still grow regularly for j values lower than the noted limiting ones. The latter is justified, since, considering e.g. constant acidity, although when colloidal $Al_2(SO_4)_3$ micelles do not form, pitting appearance is favoured with decreasing T [34], when they form θ_b

increases with decreasing T disfavouring pitting appearance; thus the decrease of T and increase of θ_b almost compensate each other. A similar behaviour is also expected at other $C_{a,0}$ values. The production of regularly grown low-p films can be thus further optimised by changing T at all $C_{a,0}$ values.

The capability to design and optimise the porous structure and mainly D_b and p at low h values which can largely vary, may also serve to aid the design of structural features of related nanomaterials, like nanotubes [15]. Further research along the lines of this work for Al anodising in H_2SO_4 baths saturated by sulfates of metals other than aluminium or other pore-forming electrolytes saturated by different salts either of aluminium or other metals could further improve the process.

Conclusions

1. The solubility of $Al_2(SO_4)_3$ in H_2SO_4 at different H_2SO_4 concentrations was determined. A minimum in the solubility appeared at H_2SO_4 concentration $C_{a,0,m} \approx 95\%$ w/v.
2. During anodising in saturated baths $Al_2(SO_4)_3$ nanoparticle micelles form in the pore base and wall surfaces/electrolyte interfaces to an extent depending on supersaturation, $C_{a,0} \leq C_{a,m}$, and unsaturation, $C_{a,0} > C_{a,m}$, conditions dominating inside pores and on h, j, T and $C_{a,0}$. Their formation is favoured by the increase of j, h and $C_{s,s}$ and decrease of T. Micelles play a critical role in the film growth mechanism and affect it in well-defined patterns. The control of this mechanism by micelles is generally more effective for $C_{a,0} \leq C_{a,m}$.
3. The average porosity of the films depends strongly on h, $C_{a,0}$, j and T; it varies with these parameters generally in a complex way and well-defined peaks are observed.
4. The critical current densities above which pitting appears are higher than those at $C_{s,s} = 0$, much more at low $C_{a,0}$ values, attributed to the fact that micelles impose a mechanism controlling regular film growth.
5. An optimisation as regards the desired porosity of regularly grown films is thus achieved. Use of ultradense baths may yield solutions for problems related to the attainment of regularly grown films with high porosity and thickness and regularly grown hard films.
6. The cited theory is of specific importance for developing new Al anodising technologies.

References

1. Leach SL, Neufeld F (1969) Corros Sci 9:225
2. Diggle JW, Downie TC, Goulding CW (1969) Chem Rev 69:365
3. Young L (1961) Anodic oxide films. Academic Press, London
4. Shreir LL (1976) Corrosion, Vol 2. Newnes-Butterworths, London
5. Smith AW (1973) J Electrochem Soc 120:1068
6. Kawai S, Ishiguro I (1976) J Electrochem Soc 123:1047
7. Rai K, Ruckenstein E (1975) J Catal 40:117
8. Chu Y, Ruckenstein E (1976) J Catal 41:384
9. Ihm SK, Ruckenstein E (1977) J Colloid Interface Sci 61:46
10. Ihm SK, Ruckenstein E (1978) IEC Prod Res Dev 17:110
11. Patermarakis G, Pavlidou C (1994) J Catal 147:140
12. Patermarakis G, Moussoutzanis K, Chandrinos J (1999) Appl Catal A General 180:345
13. Patermarakis G, Nikolopoulos N (1999) J Catal 187:311
14. Patermarakis G, Kerassovitou P (1992) Electrochim Acta 37:125
15. Li J, Papadopoulos C, Xu JM, Moskovits M (1999) Appl Phys Let 75:367
16. Thompson GE, Furneaux RC, Wood GC (1978) Corros Sci 18:481
17. Furneaux RC, Thompson GE, Wood GC (1978) Corros Sci 18:853
18. Patermarakis G, Moussoutzanis K, Chandrinos J (2001) J Solid State Electrochem 6:39
19. Patermarakis G, Chandrinos J, Moussoutzanis K (2001) J Electroanal Chem, 510:59
20. Wood GC, O' Sullivan JP (1970) Electrochim Acta 15:1865
21. Fukuda Y, Fukushima T (1983) Electrochim Acta 28:47
22. Mason RB (1956) J Electrochem Soc 103:425
23. Tajima S, Umehara Y (1981) Plating Surf Finish 68:54
24. Tomita S (1981) Alutopia 11(4):15
25. Patermarakis G, Moussoutzanis K (2002) J Solid State Electrochem 6:475
26. Patermarakis G, Moussoutzanis K (1995) J Electrochem Soc 142:737
27. Nagayama M, Tamura K (1968) Electrochim Acta 13:1773
28. Nagayama M, Tamura K (1967) Electrochim Acta 12:1097
29. Nagayama M, Tamura K, Takahashi H (1970) Corros Sci 10:617
30. Diggle JW (1973) Electrochim Acta 18:283
31. Diggle JW, Downie TC, Goulding CW (1970) Electrochim Acta 15:1079
32. Patermarakis G, Lenas P, Karavassilis Ch, Papayiannis G (1991) Electrochim Acta 36:709
33. Patermarakis G, Tzouvelekis D (1994) Electrochim Acta 39:2419
34. Patermarakis G, Moussoutzanis K (2001) Corros Sci 43:1433
35. Patermarakis G, Moussoutzanis K (2002) Corros Sci 44:1737
36. Patermarakis G, Moussoutzanis K (1995) Electrochim Acta 40:699
37. O'Sullivan JP, Wood GC (1970) Proc R Soc (London) Ser A 317:511
38. Siejka J, Ortega C (1972) J Electrochem Soc 124:883
39. Neufeld P, Ali HO (1973) J Electrochem Soc 120:479
40. Patermarakis G (1998) J Electroanal Chem 447:25
41. Patermarakis G, Karayiannis H (1995) Electrochim Acta 40:2647
42. Weast RC (ed) (1980) Handbook of chemistry and physics, 60th edn. CRC Press, Boca Raton, p E–11
43. Dodos D (1975) Electrochemical data. Elsevier, Budapest
44. Patermarakis G (1996) Electrochim Acta 41:2601
45. Ono S, Ichinose H, Masuko N (1991) J Electrochem Soc 138:3705